Chapter 5

Injection Induced Seismicity - A Thermoelastic Model

5.1 Abstract

Injection induced seismicity has been observed in several geothermal fields around the world. A favoured explanation for such earthquakes is that the overpressures generated about an injection well cause an increase in effective normal stress, $(\sigma_n + p)$, across fractures within the reservoir, making them more likely to slip (*N.B.* using tensile stress = positive, convention). However, simple scaling arguments suggest that thermal stresses might also be very significant in a geothermal environment. This paper investigates the role of advective cooling and consequent thermoelastic stressing in triggering earthquakes. A simple axisymmetric model of injection of cold water into a hot permeable fracture is considered. Heat flow within the fracture is assumed to be solely controlled by advection and outside the fracture to be purely controlled by conduction. Coupling between the temperature and pore pressure fields is neglected. The increase in σ_n induced thermoelastically is compared to the increase in fracture pore pressure for parameters appropriate to geothermal operations. We find that the thermoelastic increase in σ_n is typically greater than injection overpressure for a significant fracture area about the borehole. For a mass flow rate, $\dot{m}_{r_b}$, of 10 kg s^{-1}, water-rock temperature differences, ΔT_0, of 200°C, fault permeability thickness product, kh, of 10^{-11} m^3 and times, t, of a year or so, the thermoelastic stresses are on the order of 10 MPa for a radius of order 100 m compared to injection overpressures

on the order of 1 MPa for the same parameters. The thermal stress perturbation, $\Delta\sigma_n$, for times of interest is proportional to $\Delta T G\alpha(\kappa t)^{\frac{1}{4}}\dot{m}_{r_b}^{-\frac{1}{2}}$, where G, α, and κ are respectively the shear modulus, coefficient of thermal expansion, and thermal diffusivity. The radial dimension of the stressed zone similarly grows as $(\kappa t)^{\frac{1}{4}}\dot{m}_{r_b}^{\frac{1}{2}}$. These results are relatively unaffected by the additional complications introduced by including thermal expansion of the injected fluid or when considering a steam dominated reservoir.

5.2 Introduction

A number of studies have associated the exploitation of geothermal fields for power production with local increases in seismic activity [Majer and McEvilly, 1979; Denlinger and Bufe, 1982; Eberhart-Phillips and Oppenheimer, 1984; Sherburn, 1984; Batini *et al.*, 1985; Bromley *et al.*, 1987; Sherburn *et al.*, 1990; Stark, 1990]. These increases in seismicity are generally attributed to water injection and/or fluid extraction, the hot geothermal fluids being either steam or hot water. Of these studies only the one by Eberhart-Phillips and Oppenheimer (1984), of seismicity at The Geysers geothermal field, failed to find a significant correlation between cold water injection and seismicity. Their paper indicated that steam production was the significant controlling factor. However, a more recent study at The Geysers, using earthquake locations determined by the proprietary Unocal-NEC-Thermal network, by Stark (1990), indicates that about half the earthquakes in the field seem to be associated with cold water injection. It appears then that injection induced earthquakes are a real and significant component of commercial geothermal field seismicity.

In general, geothermal reservoirs which display induced seismicity (and a lot of those that don't) tend to be characterised by a high degree of fracture permeability. Successful geothermal production wells need to intersect one of the major high permeability fractures, to maximise extraction rates. The actual fluid volume contained within these major fractures is small and is not the principal source of geothermal fluids, rather the fracture network acts as a large exchange surface with which to tap the fluids contained in the bulk reservoir porosity. The production wells act as

pressure sinks so that during production hot water is drawn from the rock matrix porosity, down the pressure gradient, towards those fractures that are maintained at a low pressure by their connection to production boreholes. Once in the hot fracture, the fluids then flow with little impedance, via the fracture network, towards the production well. The low permeability of the rock matrix means that most of the pressure drop occurs within the rock, close to the fracture surface. If fluid pressures fall below the vapour pressure then the water will flash to steam. Hence fracture fluids can be liquid, dual phase or dry steam. The higher pressures in the rock matrix porosity though, favour storage as a dense, liquid phase.

The hot fluids flow to the surface where thermal energy is extracted. Water is left as a waste product, often containing a high concentration of the toxic materials indigenous to geothermal fluids. This waste water is disposed of by reinjection into the reservoir, returning what would be surface contaminants to their natural environment, while simultaneously helping to replenish the lost reservoir fluids. However, evaporation during the energy extraction stage means that there is a net deficit of fluid mass from the reservoir which can lead to a drying out of the reservoir. Sometimes additional surface water is added to the injectate in an attempt to make up this loss. The injection wells themselves tend to be uneconomic and disused production wells rather than purpose drilled, as the first concern in commercial geothermal operations is energy extraction.

The mechanism by which seismicity is induced by injecting fluids at above ambient pressure into fractured rock is believed to be well understood. It was originally outlined by Hubbert and Rubey [1959] and later applied to injection correlated seismicity at the Rocky Mountain Arsenal [Healy *et al.*, 1968] and Rangely Colorado [Raleigh *et al.*, 1972]. It is based on the Coulomb criterion which we express:-

$$|\tau| \leq -\mu(\sigma_n + p) + S_f \tag{5.1}$$

where τ is shear stress supported across a fracture and μ is the coefficient of friction. Here the convention, tensile stress = positive, is being used. The term in parentheses is referred to as the effective normal stress, σ_n', it is the sum of the ambient normal

stress acting on the fracture walls, σ_n, and the pore fluid pressure within the fracture, p. The cohesive shear strength of the fracture is S_f. This inequality, (5.1), defines the range of shear stress that can be supported across a fracture without it slipping. An increase in pore fluid pressure causes a larger proportion of the ambient normal stress acting across a frature to be supported by the fluid, so decreasing σ'_n. As fluids have negligible shear strength the effective shear stress supported by the frature surfaces remains unchanged. This increases the ratio of shear to normal stress, driving the fracture towards shear failure.

Little seems to be known about the effect that temperature difference between injectate and reservoir might have on stress perturbation and seismicity, although it is to be expected that injecting cold water into a hot fracture will give rise to thermoelastic stresses [*Mossop and Segall*, 1994; *Mossop and Segall*, 1995]. The flowing cold water will cool the fracture walls local to the injection well and these will respond by trying to contract. The surrounding rock will constrain this contraction and so a stress perturbation is induced. A component of this thermoelastic stress will be normal to the fracture walls and will cause an increase in σ_n and hence in effective normal stress, σ'_n. The potential for these stress perturbations to be very large is illustrated by simple scaling arguments. Assuming the simplest symmetry, the stress perturbation should be of the order $K\epsilon_{kk}$, where ϵ_{kk} is the unconstrained volume strain, and K is the bulk modulus. For an equidimensional cooled inclusion in a hot body $\epsilon_{kk} = 3\alpha\Delta T$; α is the linear coefficient of thermal expansion and ΔT is the temperature difference. Typical values for these parameters are $K = 3 \times 10^{10}$ Pa, $\alpha = 10^{-5}$, and $\Delta T = 200$ K, this means that stress perturbations on the order of 10^7 Pa or more are to be expected about injection wells, which is very substantial indeed.

In this paper we investigate the stresses induced by injecting cold water into hot fractured rock. A procedure that is commonplace in geothermal energy production and in the waterflooding of hydrocarbon reservoirs. We use a simple model to describe a single fracture and compare the perturbation in effective normal stress due to direct injectate pressure on the fracture walls, with the thermoelastic stress caused

by advective cooling. We assume that the ambient compressive stress is much larger than the stress perturbations (*i.e.*$|\sigma_n| \gg |\Delta\sigma_n|$) and hence the fracture walls are not stress free surfaces. In general we find that for realistic injection operations the injectate pressure is less significant than the thermoelastic stress, indicating that injection induced seismicity in geothermal fields is likely to be thermoelastic in origin. We go on derive a simple expression that approximates the thermoelastic stress perturbation and then to show that more complex models leave this general result unchanged.

In an effort to make this paper as clear and simple to read as possible we have made extensive use of appendices. This allows us to simply state those points that we believe are most important to the main thrust of this paper, refering the reader, who wishes to examine them more closely, to an appendix.

5.3 Setting up the Problem

We investigate the stresses about an injector using the simple model shown schematically in Figure 5-1. A fracture is represented by a uniform, thin, horizontal, permeable layer in an impermeable medium. Water is injected into this layer from the wall of an intersecting borehole, of radius r_b. Axisymmetric coordinates are used where r and z are radial and vertical distances respectively. The fault lies in the plane $z = 0$ and the borehole is centred on the line $r = 0$. Injection starts at $t = 0$, the water enters the fracture from the borehole at a mass flow rate of $\dot{m}_{r_b}$ with an initial temperature of T_{W_0}. The initial temperature of the rock is T_{R_0} and the initial fracture pore pressure is p_0. At first we neglect any phase changes and assume the water remains in a liquid state throughout the fracture, later we will consider the possibility of boiling occuring in the fracture.

The fracture itself is essentially a planar open space with multiple contact points between the two rock surfaces. It has an average aperture h. The total area of contact points is assumed to be small which is consistent with theoretical and experimental fractures under stress conditions applicable to geothermal fields [*Evans et al.*, 1992b; *David et al.*, 1994].

We begin by finding the pore pressure distribution consistent with injection at a constant mass flow rate, $\dot{m}_{r_b}$. The flow of water also cools the fault wall rock by advection and we determine how this temperature perturbation gradually penetrates into the rock matrix. We use this temperature change to calculate the thermoelastic stresses induced about the fracture. The reduction in effective normal stress due to thermoelasticity and pore pressure are then compared to give some measure of the relative importance of each.

The above scheme requires the introduction of additional parameters as we progress and some idea as to the values that they typically may have. Where this is so we choose values appropriate to an injection well in an industrial geothermal field. The variables and parameters used in this paper are given in table 5.1. We have attempted to choose values conservatively, i.e. where a range of possible values occurs we pick those that minimise thermal stresses and maximise hydraulic pressures. Similarly when assumptions are made, they are made with a typical injection well in mind. However, we believe that this analysis should be applicable to many other systems where advective cooling occurs.

5.4 Injection Induced Pressure Changes

The pore pressure in a permeable, porous, medium obeys a diffusive law, which we derive in detail in Appendix C, following [*Bear*, 1979]. For our simple model only the radial terms of the diffusion equation are important, given by:-

$$c_D \left(\frac{\partial^2 p}{\partial r^2} + \frac{1}{r} \frac{\partial p}{\partial r} \right) - \frac{\partial p}{\partial t} = 0. \tag{5.2}$$

Here the hydraulic diffusivity in the uniform fracture is given by the scalar constant c_D which can be related to the permeability, k; the dynamic viscosity, η; the fracture porosity, ϕ; and the fluid and pore space compressibilities, β_f and β_ϕ (where we have used the shorthand $\beta = \beta_f + \beta_\phi$).

$$c_D = \frac{k}{\eta \phi \beta} \tag{5.3}$$

We impose boundary conditions that dictate that the pore pressure at infinite distance remains that of the initial pore pressure p_0 and that the mass injection rate at the borehole wall is $\dot{m}_{r_b}$.

$$p(r \to \infty, t) = p_0 \tag{5.4}$$

$$q_r(r = r_b, t \geq 0) = \frac{\dot{m}_{r_b}}{2\pi r_b h}. \tag{5.5}$$

Here h is the fracture thickness and $q_r(r = r_b, t \geq 0)$ is the radial component of the fluid flux at the borehole wall once injection has started, which we define as constant. At this point we introduce Darcy's law (5.6) which is the constitutive law that relates fluid flux to pressure in permeable media,

$$\mathbf{q} = -\rho_0 \frac{\mathbf{k}}{\eta} \nabla p, \tag{5.6}$$

where ρ_0 is the reference fluid density. We use (5.6) to rewrite (5.5) as

$$\lim_{r_b \to 0} \; r_b \frac{\partial p}{\partial r}\bigg|_{r=r_b} = -\frac{\dot{m}_{r_b}\eta}{2\pi\rho_0 k h}. \tag{5.7}$$

The solution of equation (5.2) subject to (5.5) and (5.7) gives the pore pressure distribution in the fault as a function of radius and time [*Theis*, 1935],

$$p(r,t) = \frac{\dot{m}_{r_b}\eta}{4\pi\rho_0 k h} \, E_1\left(\frac{r^2}{4c_D t}\right) + p_0 \quad ; \quad r \geq r_b, \; |z| \leq h/2, \; t \geq 0 \tag{5.8}$$

where E_1 is the exponential integral of the first kind, $E_1(z) = \int_z^\infty (\exp(-t)/t)\, dt$.

Figure 5-2 is a normalised plot of pressure perturbation, $\Delta p = p - p_0$, against radial distance from the borehole. The fracture fluid pressure drops off rapidly with radial distance, behaviour that is a natural outcome of the radially divergent flow (indeed, the exponetial integral has a logarithmic type singularity at $r = 0$). We can also see from equation (5.8) that the radial distance to some chosen isobar grows in proportion to $\sqrt{t}$. This is equivalent to stating that the area of horizontal frature

containing pore pressures greater than or equal to some chosen critical value grows linearly with time.

Equation (5.8) shows that the pore pressure increase is inversely proportional to the fault permeability–thickness product, kh, *i.e.*the pore pressure increase is proportional to the hydraulic resistance of the fault. In an attempt to make the pore pressures as large as possible we have chosen a low value of kh (*i.e.*$kh = 1 \times 10^{-11}$ m^3) compared to the range displayed by typical injection wells, (e.g. for The Geysers geothermal field $kh = 1.5 \times 10^{-11}$ m^3 to 3×10^{-10} m^3, [Williamson 1990]). Pressure diffusivity in the fracture, c_D, and therefore fracture fluid pressure, are dependent on the fracture permeability, k. However, whilst the permeability–thickness product, kh, is well constrained by flow tests, the value of k is frequently uncertain. It is possible though, to estimate c_D using Kozeny's [1927] relationship between pore size and permeability, $k = s_K \phi^3/\omega^2$, where s_K is Kozeny's shape constant which has a range of 1/2 – 2/3 for high aspect ratio pores, and ω is the specific surface [*Bear*, 1979] which for a fracture we expect to be $\lesssim 4/h$. Using the Kozeny relation to eliminate porosity ϕ from (5.3) yields

$$c_D \approx \frac{(kh)^{2/3}}{\varphi \eta \beta}, \tag{5.9}$$

where φ is a dimensionless parameter of order 1–10 (generally about 2 or 3) equal to $(\omega^2 h^2/s_K)^{\frac{1}{3}}$.

Thus, for a typical permeability-thickness of $kh = 10^{-11}$ m^3 and the dynamic viscosity of water, $\eta = \eta_w$, the pressure diffusivity, c_D, is of order 1000 m^2 s^{-1}. An order of magnitude estimate is perfectly adequate, as the pressure is very insensitive to c_D. Similarly we find $\phi h \approx 7 \times 10^{-4}$ m. The porosity of the fracture itself, ϕ, we expect to be very high on the order of 1, indicating that $k \approx 10^{-8}$ m^2 and the effective fracture thickness is of the order of a millimeter. Essentially identical results are returned when using any of the various other Kozeny type relationships that have been developed theoretically and empirically [*Bear*, 1979].

Figure 5-3 shows how the pressure perturbation develops about a *typical injector*, using the parameter values from table 5.1, an injection rate of $\dot{m}_{r_b} = 10$ kg/s and

a borehole radius of $r_b = 0.1$ m. The compressibility of water is small compared to the compressibility of the fracture pore space (or the inverse of the maximum pressure perturbation) so we can use $\rho_0 = \rho_w$. The plots are for times of 10^5s, 10^6s, 10^7s and 10^8s, approximately 1, 10, 100 and 1000 days. Drops of almost 1/2 the maximum pressure perturbation are observed within the first 10 m. Maximum pressure perturbation for the parameters chosen is in the range of 2–3 MPa, and those over areas of order 10 m^2 or less.

5.5 Injection Induced Temperature Changes

To investigate the advective cooling effect in our injection model we consider the same mass injection rate, $\dot{m}_{r_b} = 10$ kg/s, and neglect fluid and pore compressibility, $\beta \to 0$. This is valid as long as $\Delta p_{\max} \ll 1/\beta$, where $\Delta p_{\max}$ is the maximum pressure perturbation, $(= p(r_b, t))$, a condition that is met for our typical injector. The initial rock temperature is uniform, T_{R_0}, the injectate enters the fracture from the borehole at a temperature of T_{W_0}. Each unit area of the fracture plane is associated with a mass, $h\phi\rho_w$, of pore fluid, which flows radially outward with velocity, $v \to \dot{m}_{r_b}/(2\pi r h \rho_w \phi)$. We assume that the fracture is thin and that the solid component of the fracture is in thermal equlibrium with the water. Thus, the problem is essentially a radial flow heat exchanger and is a specifc case of a general class of advection-diffusion problems. We solve for the approximate temperature distribution by applying to radial symmetry the method given by Carslaw and Jaegar [1959] for linear flow heat exchangers (Lauwerier [1955] gave the first solution to this linear flow problem using essentially the same approach, also see Bodvarsson [1972]).

The temperature of the rock must satisfy the heat equation

$$\nabla^2 T_R - \frac{1}{\kappa}\frac{\partial T_R}{\partial t} = 0 \tag{5.10}$$

where κ is the thermal diffusivity of the rock, and this is solved subject to the following physically constrained boundary conditions. Conservation of energy dictates that the heat flow across the rock-fracture interface must be balanced by the heat transported

away by the water and heat change in the fracture itself.

$$\xi\frac{\partial T_W}{\partial t} + v\frac{\partial T_W}{\partial r} = \frac{2\lambda}{h\phi\rho_w c_w}\frac{\partial T_R}{\partial z}\Bigg|_{z=\pm h/2} ; r > 0,\ t > 0 \tag{5.11}$$

Where λ is the thermal conduction coefficient of the rock, c_w is the specific heat capacity and the quantity ξ is a measure of the total heat contained within the fault compared to that held in the pore water alone

$$\xi = \frac{\rho_r(1-\phi)c_r}{\rho\phi c_w} + 1 \tag{5.12}$$

where ρ_r and c_r are, respectively, the density and specific heat capacity of the rock. Generally ξ will be close to 1, but we show it here for the sake of completeness. The other boundary condition requires that the temperature of the wall rock and pore water are in equilibrium at the interface.

$$T_W = T_R\Big|_{z=\pm h/2} ;\ r > 0,\ t > 0 \tag{5.13}$$

To solve this equation (5.10) subject to conditions (5.11) and (5.13), for both T_W and T_R, we have to make some simplifying assumptions. We assume the temperature to be constant across the thickness of the fracture. Within the rock matrix we assume that radial conductive heat flow, which is proportional to temperature gradient, is negligible compared to heat flow normal to the fault, (this will tend to exagerate radial thermal gradients in our solution). Lastly we assume that radial thermal conduction, in the fluid, is negligible compared to thermal advection.

Appendix D gives a detailed derivation of the temperature perturbation in the rock about the fracture, the result is

$$T_R(r,z,t) = -\Delta T_0 \,\mathrm{erfc}\left(\frac{ar^2 + b\left(|z| - h/2\right)}{\sqrt{t - Cr^2}}\right) H\left(t - Cr^2\right) +$$

$$T_{R_0} \quad ; \; r > 0, \; z \geq h/2. \tag{5.14}$$

$$\Delta T_0 = T_{R_0} - T_{W_0} \quad ; \quad a = \frac{\pi\lambda}{\dot{m}_{r_b} c_w \sqrt{\kappa}} \quad ; \quad b = \frac{1}{2\sqrt{\kappa}} \quad ; \quad C = \frac{\pi h \phi \xi \rho_w}{\dot{m}_{r_b}}.$$

As noted the pore fluid temperature, $T_W(r,t)$, is simply the same as $T_R(r, z = h/2, t)$, the rock matrix temperature at the fracture wall. The erfc term contains the details of how the the temperature perturbation varies with distance about the fracture. The heaviside function, H, merely dictates the domain over which the erfc term is valid, it is simply the radial distance the injected water front has penetrated into the fracture. This solution, (5.14), ignores the effects of fluid and fracture space compressibility, and hence is only truly valid if the maximum pore pressure perturbation (i.e. the overpressure at the bottom of the well) is small compared to the bulk modulus of the combined pore fluid, pore cavity system, i.e. $p_{max} \ll 1/\beta$. For the parameters considered here this condition is satisfied, and experimental simulations show excellent agreement with equation (5.14), [*Fitzgerald et al.*, 1997].

Figure 5-4 is a cross-section of the temperature pertubation in a vertical plane passing through the borehole for the parameters given after 100 days of injection. It shows a very thin lenticular zone of cooling about the borehole. Note the vertical exageration and hence the much greater temperature gradient normal to the fault compared to the radial component, confirming our earlier assumption that radial heat flow would be small compared to fault normal heat flow.

The temperature perturbation described by equation (5.14) is controlled by three length scales. First, there is a purely diffusive scale that describes the penetration depth of the cooling effect into the rock in the z direction, normal to the fracture plane, this is controlled by the thermal diffusivity of the rock $1/b = 2\sqrt{\kappa}$. Second, there is an advective-diffusive scale that describes the radial growth of the cooled zone, it is similarly diffusive in nature but is also dependent on the mass flow rate of

water, it's heat capacity and the thermal conductivity of the rock, this length scale is controlled by $\sqrt{1/a}$. Third, there is a purely advective scale that describes the infiltration of the injected water into the fracture, it introduces a sharp cut-off and limits the domain of cooling, it is controlled by $\sqrt{1/C}$.

To determine how the cooled zone grows with time we note that when the argument of an error function is ≥ 2 it is within 0.5% or less of its value at infinity. So by setting the argument of the error function in (5.14) equal to 2, and defining this as the boundary of the cooled zone, we can calculate that this region grows radially as

$$r_c = \frac{1}{a}\sqrt{2\sqrt{C^2 + a^2 t} - 2C} \tag{5.15}$$

and grows axially as

$$z_c = \frac{2\sqrt{t}}{b}. \tag{5.16}$$

At times, $t \ll C^2/a^2$, radial growth of the cooled zone is limited by advection and grows as $\sqrt{t/C}$. At longer times, $t \gg C^2/a^2$, the fluid injection front extends well beyond the cooled zone, and the radial growth of the cooled zone becomes controlled by the slower moving advective-diffusive properties of the system, so that it grows as $t^{\frac{1}{4}}/\sqrt{a}$. At this stage, $t \gg Cr^2$ for all r of interest, *i.e.*all r within the cooled zone, and (5.14) may be simplified to

$$\begin{aligned} T_R(r,z,t) &= T_{W_0} + \Delta T_0 \operatorname{erf}\left(Ar^2 + B\,|z|\right). \\ A &= \frac{a}{\sqrt{t}} \quad ; \quad B = \frac{b}{\sqrt{t}} \end{aligned} \tag{5.17}$$

in agreement with the finding of Bodvarsson [1972].

Equation (5.17) is a good approximation to (5.14) for the time domain $t \geq 3Cr_c^2$, which is equivalent to $t \geq 24C^2/a^2$. To derive this latter inequality, simply substitute $t = nCr_c^2$, where $n > 1$, into equation (5.15), which leads to $r_c^2 = 4(n-1)C/a^2$, and hence $t = nCr_c^2 = 4n(n-1)C^2/a^2$. For the parameters we're using here equation

(5.17) is valid for times of order 100 seconds or more, and so equation (5.17) is relevant to the time scale at which injection induced seismicity occurs.

The cooled zone grows axially with $\sqrt{t}$, (5.16), whereas the radial growth is proportional to $t^{1/4}$. This means that the radial growth of the cooled zone becomes proportionally slower than the axial growth causing the cooled zone to become spheroidal, which violates the assumption that $\partial T/\partial z \gg \partial T/\partial r$. However, the aspect ratio of the cooled zone doesn't reach unity, *i.e.*$r_c \approx z_c$, until 20,000 years or so, for our typical parameters, which makes it of little concern here. The time period for which equation (5.14) is valid is more thoroughly investigated later in the paper (in Appendix G.1).

5.6 Thermoelastic Stresses

Thermoelasticity is a specific case of a general family of analogous body forces obeying a scalar potential gradient law (e.g. poroelasticity). In general the stress state can be found by convolving the inducing function, in this case the temperature, T (where $T(r,z) = T_R(r,z) - T_{R_0}$), with appropriate Green's functions.

$$\Delta\sigma_{ij}(\mathbf{x}) = \int_V T(\mathbf{y})\sigma^*_{ij}(\mathbf{x};\mathbf{y})dV \tag{5.18}$$

The V denotes the volume of interest, σ_{ij} is the stress tensor and σ^*_{ij} are the stress Green's functions. In Appendix E we show how the stress Green's functions are derived. However, these yield integrals, of the form equation (5.18), that are non-trivial and need to be evaluated numerically. This in itself is problematic, as the Green's functions σ^*_{ij} display hypersingular behaviour so that direct numerical integration is inappropriate.

The problem of hypersingularity was resolved by exploiting the fact that the temperature perturbation, $T(\mathbf{y})$, must be a solution to the heat equation (5.10) and is therefore smooth and falls to zero at infinite distance. This allows us to trade-off integration of the hypersingular Green's functions (a smoothing operation) against differentiation of the temperature function (a roughening operation). Integration by parts allows equations (5.18) to be recast in the form (5.19)

$$\Delta\sigma_{ij}(r,z) = \int_{\zeta}\int_{\varrho} \frac{\partial^2 T(\varrho,\zeta)}{\partial\varrho\partial\zeta}\tau^*_{ij}(r,z;\varrho,\zeta)d\varrho d\zeta. \tag{5.19}$$

The appropriate modified (smoothed) Green's functions are denoted as $\tau^*_{ij}(r,z;\varrho,\zeta)$. They have logarithmic order singularities which do not cause problems for direct numerical integration. These modified Green's functions and equations (5.19) are derived in Appendix F. They can be used to determine the stress perturbation tensor at any point due to an axisymmetric temperature disturbance. We will restrict ourselves in this paper to considering $\Delta\sigma_n$ at the fracture surface, $z \to 0$, but have included all the Green's functions components for all z in Appendix F for the sake of generality, and in the hope that they will be found useful.

The increase in normal stress across the fracture, *i.e.*the opening stress perturbation $\Delta\sigma_n$, due to thermoelastic stressing of the rock can be found directly from the fracture normal component of the stress tensor, σ_{zz}. This then leads to an equal increase in σ'_n and is directly comparable to the increase pore fluid pressure, Δp. (Note we are assuming that the ambient compressive stress is large compared to the tensile stress perturbations, $|\sigma_n| \gg |\Delta\sigma_n|$, so that the fracture does not act as a stress free surface).

The thermoelastic reduction in σ_n is shown in figure 5-5 for the same parameters and times as in figure 5-3. They have maxima at $r = 0$, where the cooled zone has penetrated deepest into the rock. These maxima are broad and roughly Gaussian in shape. The radial distance over which a reduction in fault normal compression, $\Delta\sigma_n > 0$, is observed approximates that of the cooled zone described above (roughly $r_c/2$). Beyond this $\Delta\sigma_n$ changes sign and becomes compressional, this is to be expected for an internal source of stress, for which the net force across the plane $z = 0$ must be zero. Note that for our typical injector the thermoelastic reduction in σ'_n is much greater than the maximum pore pressure local to the borehole. The indication is that, for a typical injection well in a geothermal field, thermoelastic stress perturbations are larger in magnitude than injection overpressure for significant fracture areas about the borehole. Hence it seems more likely that injection induced seimicity in hot fractured

rock is controlled by thermal stresses than injection pressures, although pore pressure effects may be non-negligible.

5.7 A Closed Form Estimate

The numerical solutions are not particularly straightforward and any simple relationship between the stress perturbation and the controlling parameters has become obscured. The solutions shown in figure 5-5, show clear signs of similarity and simple scaling with time. It is therefore desirable to have a closed form estimate of the thermoelastic reduction in σ_n' to investigate these relationships.

We begin by approximating the temperature perturbation as

$$T_R(r,z,t) \approx T_{R_0} + (T_{W_0} - T_{R_0}) \exp\left[-2Ar^2\right] \operatorname{erfc}\left[B|z|\right]. \tag{5.20}$$

This provides a reasonable fit to equation (5.17), the comparison between the two functions is shown in figure 5-6, and more importantly the spatial derivatives are similar.

We insert (5.20) and the stress Green's function σ_{zz}^* from equation (F.5) in Appendix F into equation (5.18) to gain the following integral for the approximate stress change, $\tilde{\sigma}_{zz}(r,0,t)$

$$\begin{aligned}\Delta\tilde{\sigma}_{zz}(r,0,t) &= 2\Delta T G \aleph \int_0^\infty \left\{ \frac{1}{4A} \exp\left[\frac{-k^2}{8A}\right] \right. \\ &\qquad \left. \left(1 - \exp\left[\frac{k^2}{4B^2}\right] \operatorname{erfc}\left[\frac{k}{2B}\right]\right)\right\} kJ_0(kr)dk. \end{aligned} \tag{5.21}$$

Here G is the rock shear modulus; the variable $\aleph = \alpha(1+\nu)/(1-\nu)$ where α is the linear coefficient of thermal expansion for the rock and ν is Poisson's ratio. This is simply the zero'th order Hankel transform of the term contained in braces. The next step is to expand the term in parentheses into a series

$$\left(1-\exp\left[\frac{k^2}{4B^2}\right]\operatorname{erfc}\left[\frac{k}{2B}\right]\right)=\sum_{i=1}^{\infty}\left[\frac{k^{2i-1}(i-1)!}{\sqrt{\pi}B^{2i-1}(2i-1)!}-\frac{k^{2i}}{B^{2i}2^{2i}i!}\right], \tag{5.22}$$

which allows the integral in equation (5.21) to be evaluated

$$\begin{aligned}\Delta\tilde{\sigma}_{zz}(r,0,t) &= \Delta TG\aleph\sum_{i=1}^{\infty}\frac{2^iA^{i-\frac{1}{2}}}{B^{2i}}\left[\sqrt{2}B\ {}_1F_1\left(i+\frac{1}{2},1,-2Ar^2\right)\right.\\ &\left.-2\sqrt{A}\ {}_1F_1\left(i+1,1,-2Ar^2\right)\right],\end{aligned} \tag{5.23}$$

where ${}_1F_1$ is the confluent hypergeometric function of the first kind. This series solution, equation (5.23), can now be used to explore some of the properties of the thermal stress perturbation.

We first explore the maximum stress perturbation, which occurs at $r = 0$. Note that ${}_1F_1(c_1, c_2, 0) = 1$, for all values of c_1 and c_2. So that, for $r = 0$, the series in (5.23) converges exactly to

$$\Delta\tilde{\sigma}_{zz}(0,0,t)=\Delta TG\aleph\frac{2\sqrt{2A}}{\sqrt{2A}+B}. \tag{5.24}$$

for all values of A and B. Recall that $\sqrt{1/A}$ is the radial length scale of the cooled zone and $1/B$ is its axial length scale. Since the estimated temperature perturbation is only applicable for times when the cooled zone is still very thin (100's of seconds to thousands of years for our typical parameters), then we know the radial length is much less than the axial length, for all times of interest. Hence we can further approximate (5.24) as

$$\begin{aligned}\Delta\tilde{\sigma}_{zz}(0,0,t) &\approx \Delta TG\aleph\frac{2\sqrt{2A}}{B}\\ &\approx \Delta TG\aleph\sqrt{\frac{32\pi\lambda\sqrt{\kappa t}}{\dot{m}_{r_0}c_w}}.\end{aligned} \tag{5.25}$$

The peak stress perturbation at $r = 0$ (5.25) increases with $(\kappa t)^{\frac{1}{4}}$, the square root of the purely diffusive length scale, and $1/\sqrt{\dot{m}_{r_b}}$. This latter scaling relationship seems somewhat counterintuitive, in that lower injection rates lead to greater stress perturbations. However, this result becomes more understandable when we consider the analagous Eshelby inclusion problem [*Eshelby*, 1957] in the Discussion section below.

We now consider the radial extent of the stress perturbation. To evaluate equation (5.23) at $r > 0$ requires that $\sqrt{2A}/B \ll 1$, *i.e.*that the cooled zone is thin as was assumed in calculating the temperature perturbation in the first place. If this is true then the series in (5.23) converges rapidly and only the $i = 1$ term need be considered. An excellent fit to the numerical results is found from this approximation (figure 5-7a). However, the ${}_1F_1\left(3/2, 1, x\right)$ term dominates ${}_1F_1\left(2, 1, x\right)$ leading to an even simpler approximation

$$\Delta\tilde{\sigma}_{zz}\left(r, 0, t\right) \approx \Delta T G \aleph \frac{2\sqrt{2A}}{B}\, {}_1F_1\left(\frac{3}{2}, 1, -2Ar^2\right). \tag{5.26}$$

For the approximation in (5.26) to be valid $\sqrt{2A}/B \ll 1$, which we rewrite as $t \lll (1/\kappa)(\dot{m}_{r_b} c_w)^2/(8\pi\lambda)^2$, equivalent to $t \lll 10^{11}$ s, for our typical injection parameters. Agreement of equation (5.26) with the full numerical thermoelastic stress calculation is shown in figure 5-7b. The fit is close and is achieved with a significant reduction in computation. (Note also that equation (5.26) can be expressed using the more familiar modified Bessels functions of the first kind ${}_1F_1\left(3/2, 1, x\right) = \exp\left(x/2\right)\left(\left(1 + x\right) I_0\left(x/2\right) + x I_1\left(x/2\right)\right)$, though less succinctly).

We use equation (5.26) to approximate the extent of the tensile stress perturbation, which can be found from the estimate of the first zero, r_0, of ${}_1F_1\left(3/2, 1, -2Ar^2\right)$. Following Abramowitz and Stegun [1965, sec. 13.7.2] we find

$$r_0 \approx \frac{3}{8}\sqrt{\frac{\pi \dot{m}_{r_b} c_w \sqrt{\kappa l}}{2\lambda}}. \tag{5.27}$$

Thus the radial extent of the tensile stress perturbation increases with $t^{\frac{1}{4}}$ and with

$\sqrt{m_{r_b}}$. These scaling relationships are in agreement with the radial growth of the thermal perturbation described by equation (5.17) as we would predict.

5.8 Discussion

We are assuming here that for injection induced seismicity the permeable fractures and the rupture surfaces are the same entity. This seems reasonable as we expect the seismic slip to occur on fracture surfaces that are closest to where pressure and fluid flow is greatest. We also note that most of the seismic studies are recording earthquakes with magnitudes of > 0, equivalent to source dimensions of > 100 m^2 [*Abercrombie & Leary*, 1993]. This suggests a large fracture surface is involved. As we assume large fractures are relatively rare the simplest conclusion is that the conductive and slipping fractures are one and the same. If this is the case then the stress perturbation of importance for earthquake triggering is that in the effective normal stress $\Delta\sigma'_n$, whether it is induced by hydraulic pressure Δp or thermoelastic stressing $\Delta\sigma_n$. Both perturbations are directly comparable, and neither hydraulic pressure or thermoelastic stress induces any change in shear stress across the fracture. Further work is needed to examine slip on neighboring fractures, which would in general be subject to both changes in normal and shear stress.

Hydraulic pressures are generated by the flow impedance of the fracture. As the flow diverges away from the borehole, fluid flux drops steeply and pressure similarly falls rapidly with distance. Therefore high overpressures only occur very close to the borehole. In operational geothermal fields injection overpressures are seldom great as water is returned to the reservoir as cheaply as possible, precluding the use of expensive pumps. For steam dominated reservoirs injection is usually driven simply by the head of water in the injection well.

The thermoelastic stresses are generated by the formation of a cooled volume of rock about the fracture, close to the injection well. The cooled zone contracts and the constraint of the surrounding rock induces stress. This scenario is analogous to Eshelby's problem [*Eshelby*, 1957], where he calculated the elastic response due to the uniform expansion or contraction of an ellipsoidal domain in a full space. His results

for an oblate spheroidal inclusion that is uniformly cooled, sitting in a warm infinite substrate, show that the tensile stress perturbation developed along its minor axis is inversely proportional to its aspect ratio (where aspect ratio is defined as: major axis length / minor axis length). Hence, as the cooled zone described by equation (5.17) becomes more spherical in shape we would expect $\Delta\sigma_n$ to increase. The reduction in aspect ratio of the cooled zone in equation (5.17) can be seen to scale with $t^{\frac{1}{4}}$ and $1/\sqrt{\dot{m}_{r_b}}$, which agrees with the scaling observed in the stress perturbation $\Delta\sigma_n$ given by equation (5.26). (N.B. an order of magnitude estimate of $\Delta\sigma_{zz}(r=0,z=0)$ can be found by approximating the temperature perturbation, equation (5.17), as an infinite series of nested, progressively cooler, best fitting ellipsoids, and then solving for the summed stress perturbation at $r=0,z=0$).

The possibility of the aspect ratio of the cooled zone being < 1 for equations (5.14) and (5.17) is merely an artifact due to ignoring radial heat diffusion. In reality this can never happen and an aspect ratio of 1 is the physical limit that can be achieved. Moreover, our analysis requires apsect ratios $\gg 1$, to be valid and is not reliable outside this limit.

In figure 5-8 we show how the peak stress perturbations and hydralic pressures vary with injection rate and permeability-thickness of the fracture. We choose these two parameters because they will vary the most between injection wells. The dashed lines indicate the peak thermoelastic stress perturbation, $\Delta\sigma_n$, as a function of mass flow rate, $\dot{m}_{r_b}$, for a temperature difference $\Delta T_0 = 100$ K, all other parameters as table 5.1, at $10^5, 10^6, 10^7$ and 10^8 seconds. The solid lines give the maximum hydraulic pressure, $\Delta p_{\max} = \Delta p(r = r_b)$, as a function of $\dot{m}_{r_b}$ for a range of plausible permeability-thickness values, kh, for the same times, again all other parameters as table 5.1. As expected the hydraulic pressures dominate for high flow rates and tight fractures, but the fact that injection pressure is limited by the economics of pumping means that they will rarely exceed the order of 10 MPa. The thermal stresses tend to dominate for low to moderate injection rates into relatively permeable fractures, they also grow far more rapidly with time, $\propto t^{\frac{1}{4}}$, compared to the logarithmic growth of hydraulic pressure. The thermoelastic stress perturbation scales directly with ΔT_0 so it is simple to interpret the results for other temperature differences. However, care should be

taken when extrapolating form figure 5-8 for lower flow rates and longer times than shown as the assumption of a thin cooled zone starts to break down beyond the limits in the figure.

The dependence of the stress perturbation on the aspect ratio of the cooled zone leads to a counter-intuitive prediction. If cold water injection is stopped after some period of time, the aspect ratio of the cooled zone will at first decrease even more rapidly than while injection was occuring. *i.e.*the axial distance to a given isotherm will still continue to grow due to thermal diffusion but the radial growth, which is contolled by fluid flow will stop. The cooled zone will hence tend to become more spherical at first. Therefore after injection is stopped, the fracture normal thermoelastic stress perturbation will initially increase, whereas hydraulic pressures in the fracture will drop instantaneously. Of course thermal diffusion will eventually remove the temperature and stress perturbation but this will take time of the same order that the cooled region was created in. Hence, the prediction is that hydraulically induced seismicity should cease rapidly after injection stops, whereas thermoelastically induced seismicity should continue for some time after. Evidence for such behaviour is found for injection wells at The Geysers, where occasional cessation of injection sometimes leads to apparent increases in seismicity, contrary to what would be expected for a purely pressure driven process [Chapter 2]

Real injection conditions are more complex than the simple model that we have solved for here. In Appendix G we try to show how the stress perturbation $\Delta\sigma_n$ will be affected when we relax some of the assumptions and simplifications that we have made. Specifically we investigate the valid time domain of our thermal model, the role of the thermal expansion of the injected water, steam filled fractures, injectate boiling and sloping fractures.

We find that the assumptions made to estimate the temperature are valid at any time of practical interest for all reasonable injection scenarios (from seconds to hundreds of years). Typically for the other questions we can do little more than give upper bounds on the influence these will have on $\Delta\sigma_n$. However, these bounds show that we are only introducing second order changes in the thermoelastic stresses as we consider more complex injection scenarios, and injections overpressures are

often actually reduced. Hence we find repeated confirmtion that thermal stresses are the dominant stress perturbation for realistic injection operations into a fractured geothermal reservoir.

It should be emphasised that thermoelastic stressing is a real and well known phenomenon. It is almost inescapable that pumping cold water through hot rocks will induce significant stress perturbations. If we consider the shape of the cooled inclusion formed about a fracture then we find that it's dimensions are strongly constrained. Conservation of energy dictates that the volume integral of the temperature perturbation is independent of the detailed temperature distribution. The result that the cooling effect penetrates into the fracture walls a distance of length scale $\sqrt{\kappa t}$ is a robust result, insensitive to any model subtleties, so that the fracture normal length scale of the cooled zone is invariant. The areal infiltration of the injected water is dependent only on injection rate and fracture aperture, if these remain constant then the area of fracture contained within the cooled zone is also invariant to flow details. Eshelby inclusion theory for an ellipsoid finds that the stress perturbation along the minor axis is at a minimum if the major and intermediate axis are equal in length. Therefore the indication is that the maximum value of $\Delta\sigma_n$ close to the borehole will be at least the same as the radially symmetric case, whatever the actual fracture flow details are and that the surface area of fracture effected will also be conserved for a range of flow geometries. The magnitude and area of thermal stress perturbation is therefore a strongly conserved feature and it is difficult to see how it can fail to exist. Only where fractures are of very low permeability and high pressure pumping is required, does it seem likely that thermal stress perturbations will fail to predominate over injection pressures in a geothermal setting, over realistic time periods.

The conclusion that thermoelastic effects can dominate stress changes about an injection well has profound importance for any injection operation where the reduction in σ_n' is a concern. In this paper the motivation has been the effect on induced seismicity. Equally though, operations such as well stimulation by injection, or hydraulic stress characterisation, rely on understanding how σ_n' varies spatially and temporally during injection. Throughout we have assumed that fracture permeability is uncoupled from fracture normal stress, this is clearly a simplification, though justifiable

considering our assumption that $\Delta\sigma_n \ll \sigma'_n$. However, it is easy to see how fracture normal stress increases could lead to fracture opening and provide a mechanism for increasing permeability of already moderately permeable fractures. For cases where the temperature difference between rock and injectate is small or where the hydraulic conductivity is low then thermoelasticity can safely be ignored. However, where there are large temperature differences and moderate fracture conductivities thermoelastic effects will be of increasing importance. The possibility that thermal effects could contribute to the opening stresses determined by hydraulic stress tests, has been suggested by Cornet *et al.*[1997]. They note an instance where a high flow rate hydraulic stress test in the Soultz geothermal field yields a value of σ_n that appears to be impossibly low.

5.9 Conclusions

Injection induced seismicity is often ascribed to the reduction in effective normal stress, σ'_n, due to the necessary overpressure required to force injectate into rock fractures. However, we have shown that for a fracture in a geothermal reservoir the reduction in σ'_n due to thermal advection by the injectate, can be much larger than that due to elevated pore pressure. The magnitude of this thermoelastic reduction scales with the temperature difference between the rock and the injected water, the rock stiffness, and the coefficient of thermal expansion. The area of fracture influenced by thermal stresses grows with $\dot{m}_{r_b}\sqrt{t}$ (after an initial growth stage that scales with t). Similarly the magnitude of the reduction in σ'_n grows with $\sqrt{\sqrt{t}/\dot{m}_{r_b}}$. In comparison the hydraulic pressure scales with $\ln t$ and the fault area effected grows linearly with time. This suggests that we could distinguish between pressure and thermal effects by the growth of seismicity in time. However, this simple analysis assumes a close to neutral buoyancy of the injectate and ignores the possible complexities of real fracture networks. We suggest that the continued triggering of seismicity after cold water injection has stopped may provide a better test. Hydraulic overpressures in the fracture start to drop in the fracture as soon as injection ceases, hence if seismicity is hydraulically induced it should rapidly diminish, if seismicity is thermally

induced then it should initially increase after injection stops. Observations at The Geyers geothermal field show continued seismicity following the cessation of injection [Chapter 2], supporting the contention that thermal stresses are significant.

α	Linear Coefficient of Thermal Expansion for Rock	10^{-5}
α_w	Linear Coefficient of Thermal Expansion for Water	10^{-3}
β_f	Compressibility of Water	4×10^{-10} Pa^{-1}
β_{fs}	Compressibility of Steam	$\sim 4 \times 10^{-7}$ Pa^{-1}
β_ϕ	Compressibility of Pore Space	3×10^{-8} Pa^{-1}
η_s	Dynamic Viscosity of Steam	$\sim 10^{-5}$ kg m^{-1} s^{-1}
η_w	Dynamic Viscosity of Water	10^{-3} kg m^{-1} s^{-1}, @ 20 °C
		10^{-4} kg m^{-1} s^{-1}, @ 200 °C
κ	Thermal Diffusivity of Rock	10^{-6} m^2 s^{-1}
λ	Thermal Conductivity of Rock	2 W m^{-1} K^{-1}
ν	Poisson's Ratio for Rock	0.25
ρ_0	Density of Water	1000 kg m^{-3}
ρ_s	Density of Steam	10 kg m^{-3} @ $\sim 10^6 - 10^7$ Pa
ρ_r	Density of Rock	2700 kg m^{-3}
ϕ	Porosity of Fracture	$\sim 0.3 - 1.0$
c_w	Specific Heat Capacity of Water	4200 J kg^{-1} K^{-1}
c_r	Specific Heat Capacity of Rock	1000 J kg^{-1} K^{-1}
kh	Permeability Thickness Product	10^{-11} m^3
$\dot{m}_{r_b}$	Mass Injection Rate	10 kg s^{-1}
r_b	Borehole Radius	0.1 m
G	Shear Modulus of Rock	2×10^{10} Pa
K	Bulk Modulus of Rock	3.3×10^{10} Pa
T_{R_0}	Initial Rock Temperature	240 °C
T_{W_0}	Initial Rock Temperature	40 °C

Table 5.1: Typical parameters used to illustrate this paper

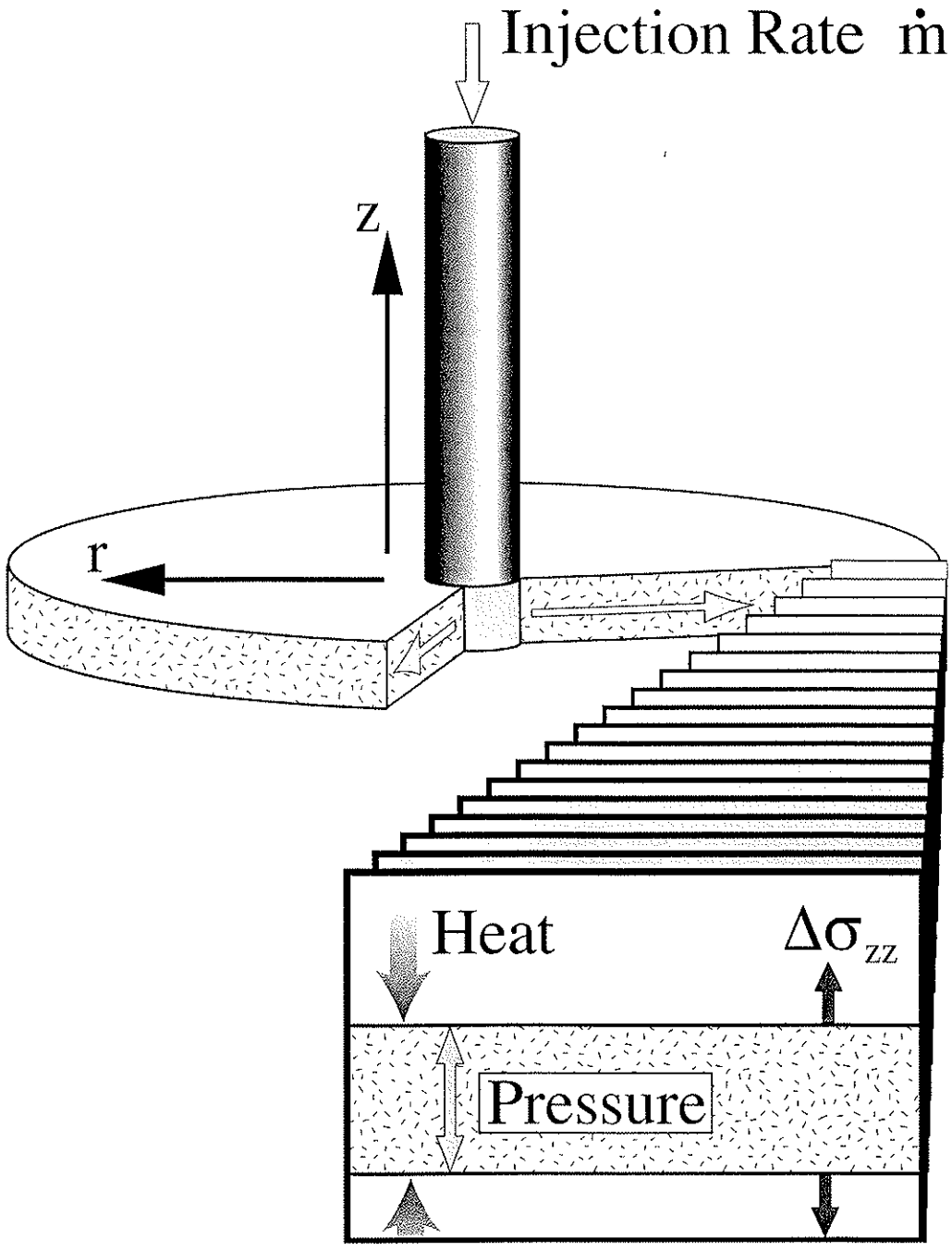

Figure 5-1: Schematic diagram of the simple injection model. Origin is at the centre of the borehole, in the middle of its intersection with the fracture.

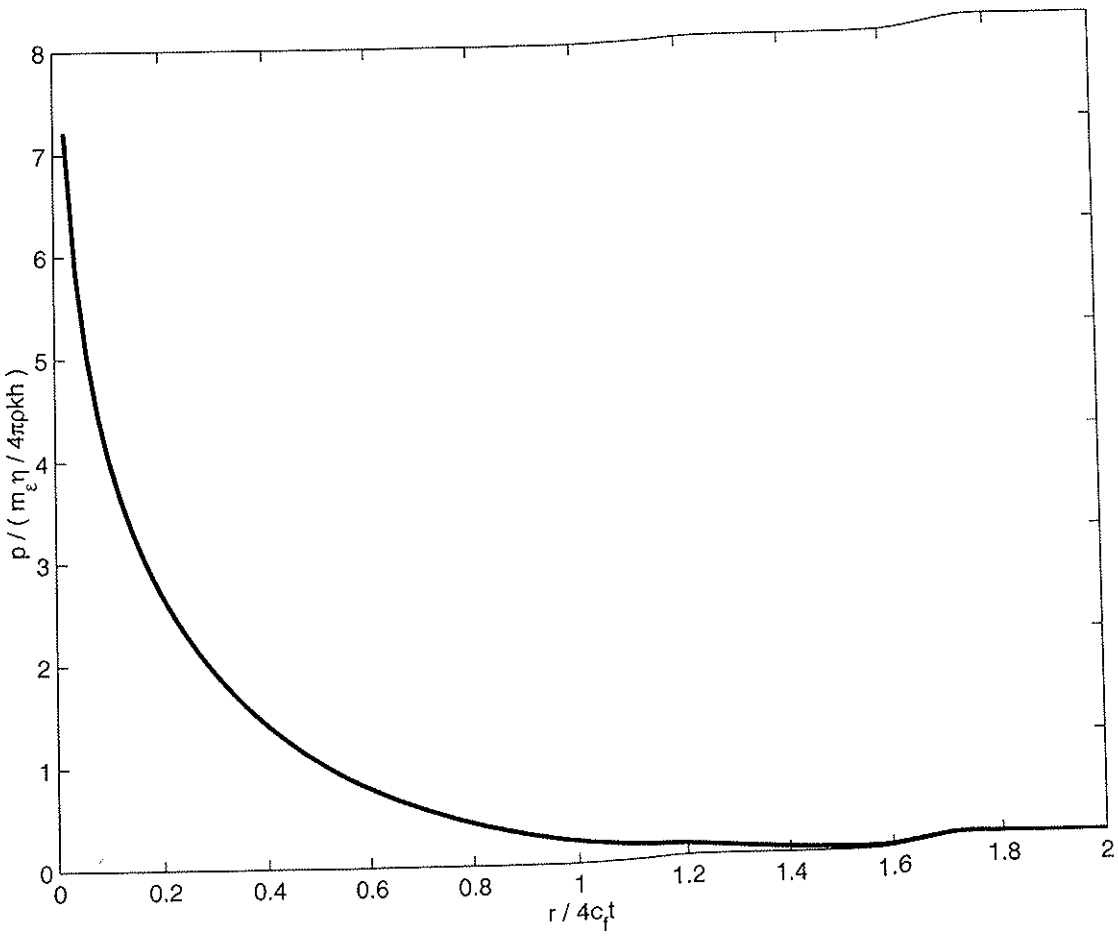

Figure 5-2: Plot of normalised pressure against normalised radius. Note logarithmic singularity at $r = 0$

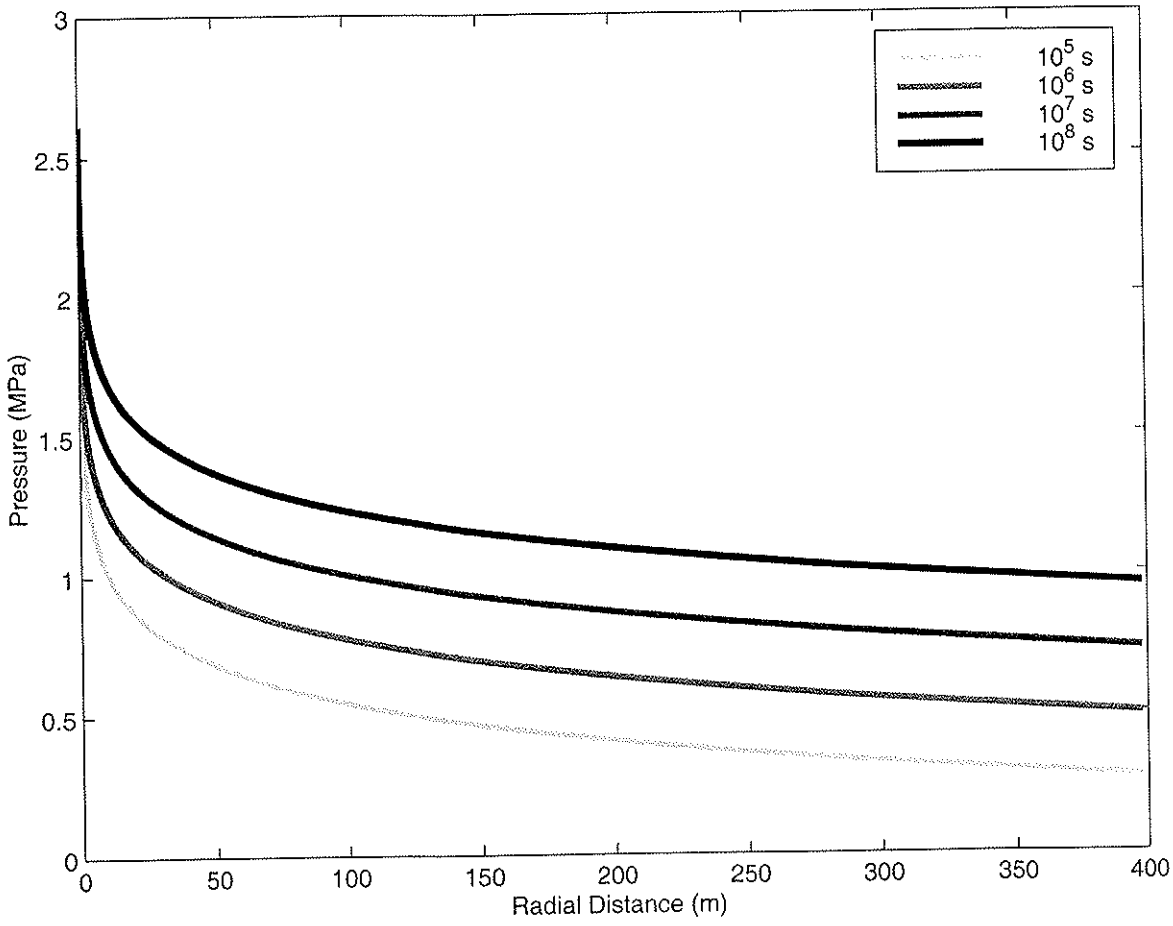

Figure 5-3: Pressure radius relationship for our typical injector (see table 5.1 for parameters). Note that maximum pressures at $r = r_b = 0.1$ m are shown.

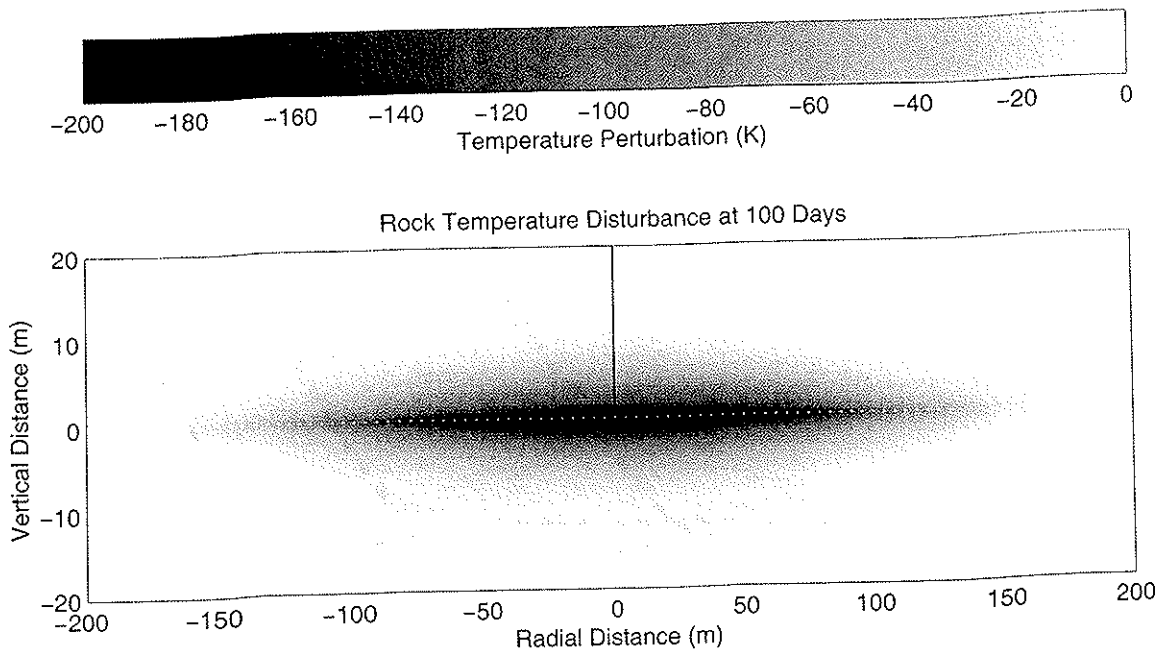

Figure 5-4: Plot of temperature perturbation after 10^7 s ($\approx$ 100 days), of injection for our typical injector.

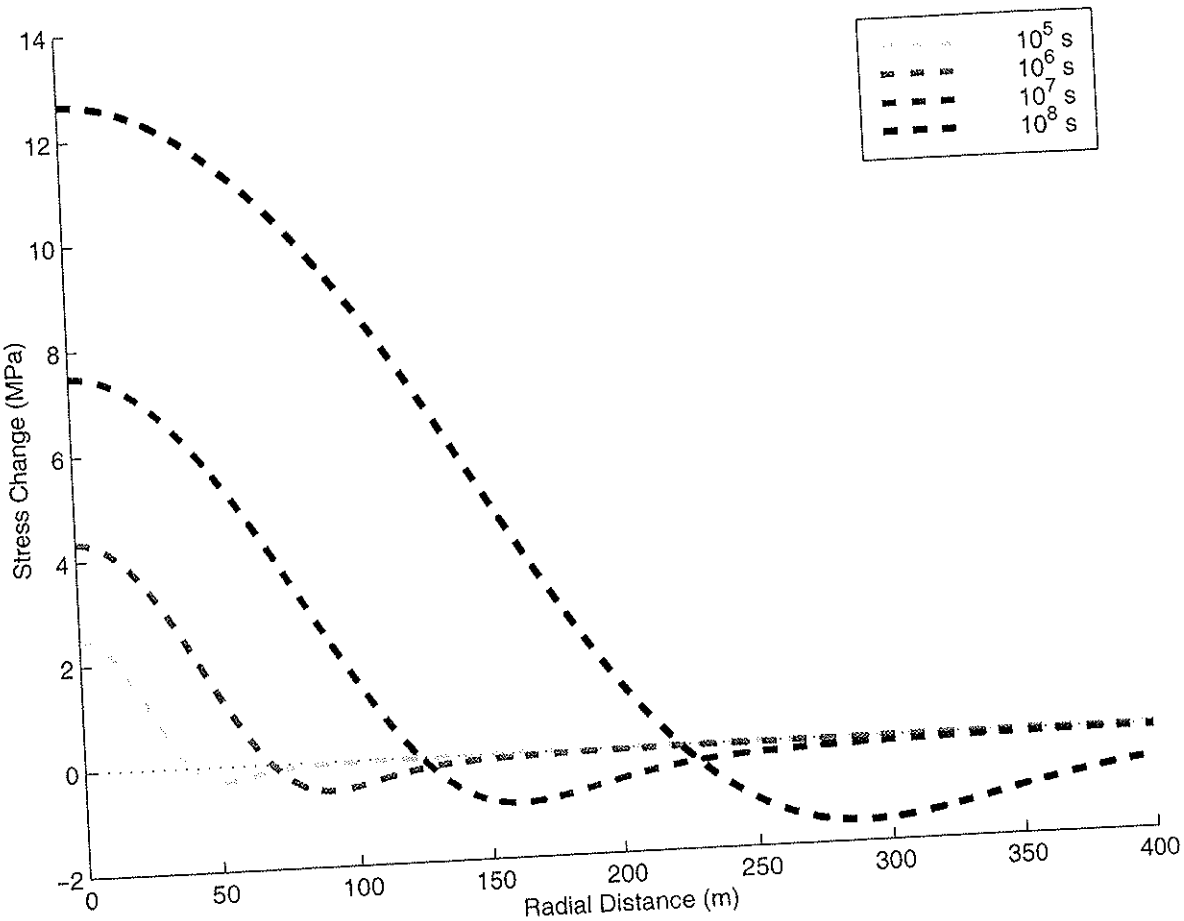

Figure 5-5: Thermoelastic reduction in σ_n for our typical injector for 10^5–10^8 seconds, approximately 1–1000 days.

(a)

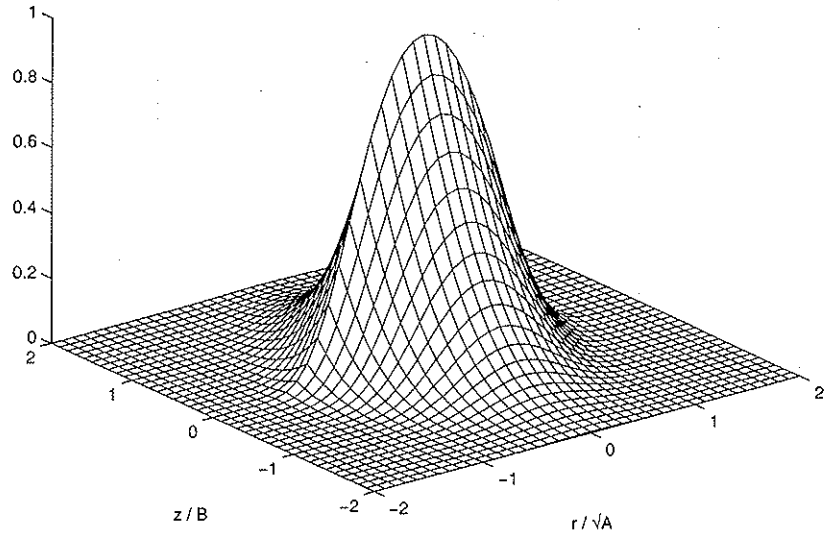

(b)

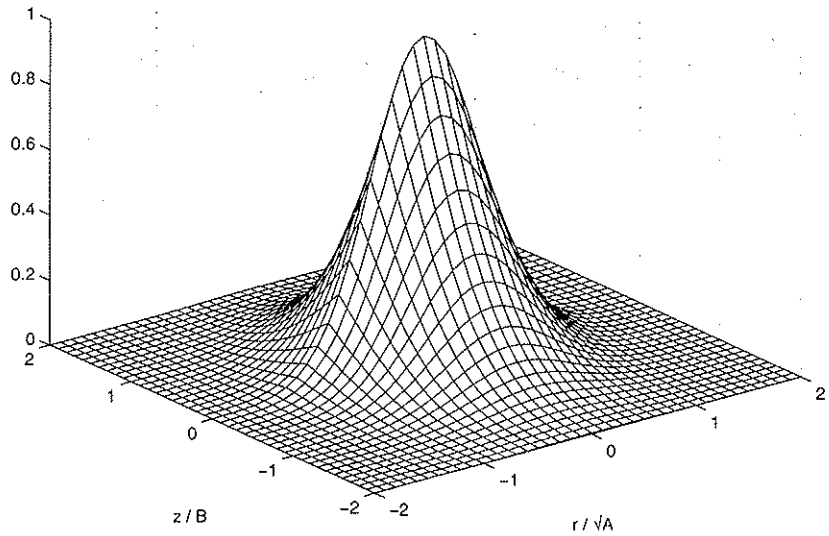

Figure 5-6: (a) Normalised plot of the function $T = \mathrm{erfc}\,(Ar^2 + B\,|z|)$; (b) Normalised plot of the function $T = \exp(-2Ar^2)\,\mathrm{erfc}\,(B\,|z|)$.

(a)

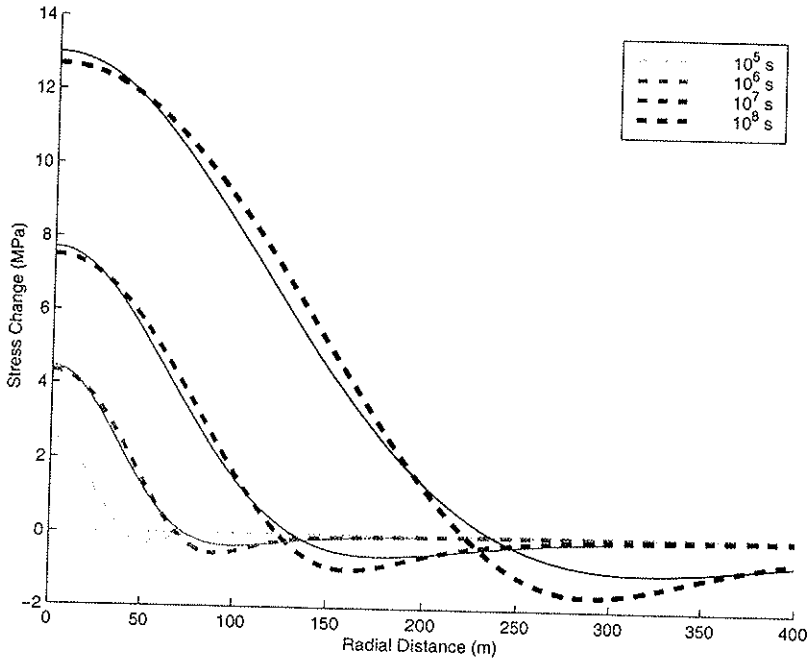

(b)

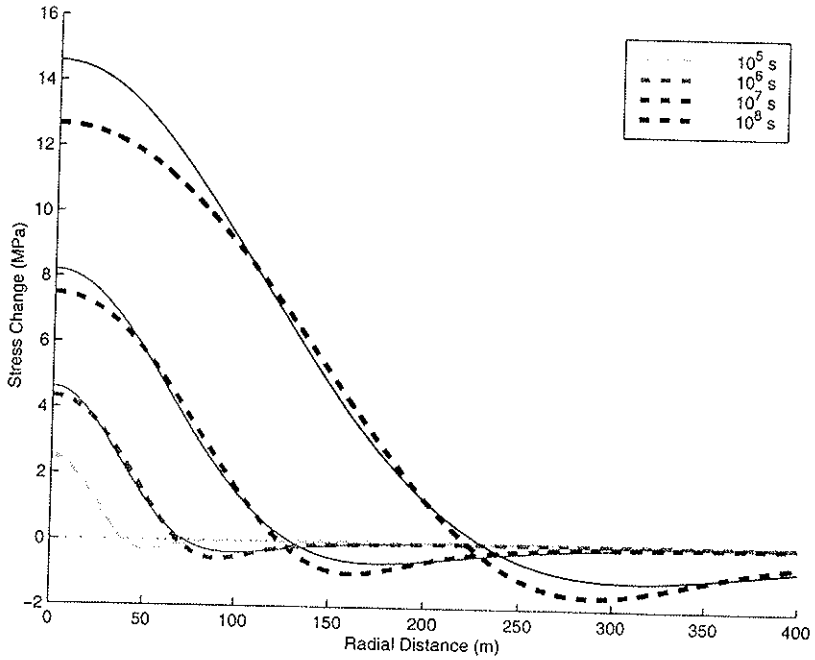

Figure 5-7: Comparison between numerically solved and closed form estimates of thermoelastic reduction in σ_n for our typical injector, the closed form estimate is shown as the thin solid line and the numerical solution is the thicker dashed line. (a) Closed form estimate is given by the first member of the series in equation (5.23), *i.e.*the $i = 1$ term. (b) Closed form estimate is given by equation (5.26).

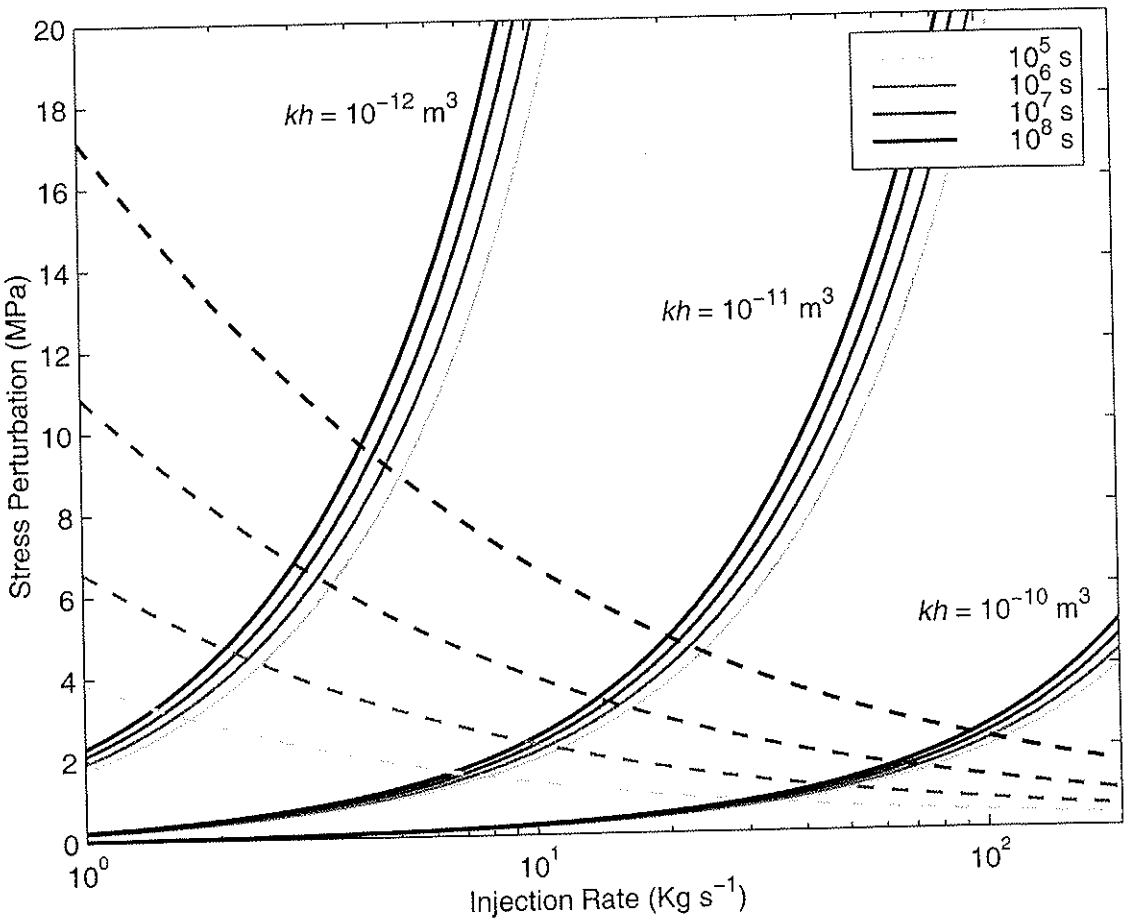

Figure 5-8: Maximum hydraulic pressure, $p(r = r_b)$, shown as solid lines, and thermoelastic stress perturbation, shown as dashed lines, as a function of mass injection rate. Injection times are indicated by the line colour. A range of permeability-thickness values are shown, $kh = 10^{-12}, 10^{-11}$ and 10^{-10} m^3, that effect hydraulic pressure. The initial temperature difference between the injected water and the rock is, $\Delta T_0 = 100$ K, the thermal stress perturbation scales linearly with ΔT_0. All other parameters are as shown in table 5.1.

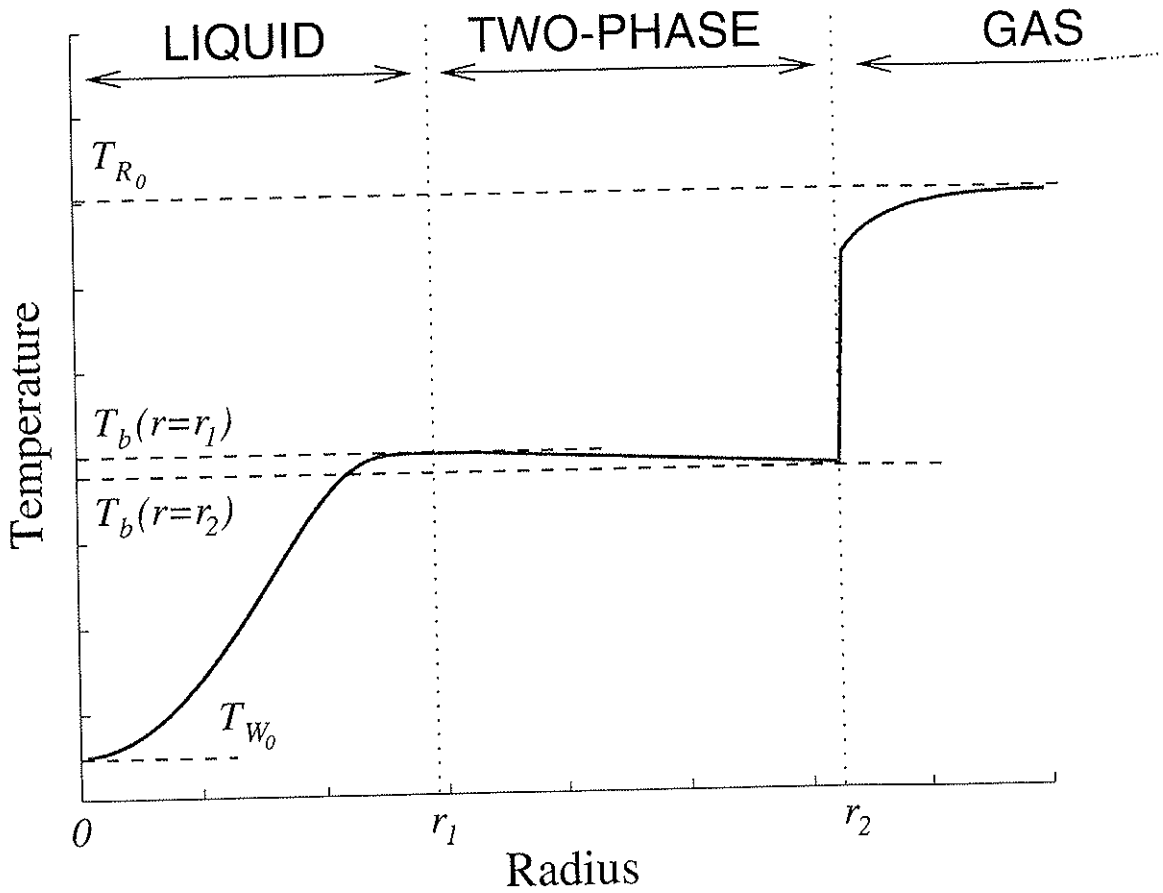

Figure 5-9: Schematic diagram of the temperature function developed by a cold injected liquid, spreading radially in a hot fracture where it is heated beyond its boiling point.

Appendix D

Deriving the Temperature Perturbation

We assume that radial heat flow is negligible compared to fracture normal heat flow so equation (5.10) can be written:-

$$\frac{\partial^2 T_R}{\partial z^2} - \frac{1}{\kappa}\frac{\partial T_R}{\partial t} = 0. \tag{D.1}$$

This is then subject to boundary conditions dictated by conservation of energy across the fracture wall and temperature continuity across the fracture wall (equations (5.11) and (5.13) respectively)

$$\xi\frac{\partial T_W}{\partial t} + v\frac{\partial T_W}{\partial r} = \frac{2K}{h\phi\rho_w c_w}\frac{\partial T_R}{\partial z}\Bigg|_{z=\pm h/2}; \quad r > 0,\, t > 0 \tag{D.2}$$

$$T_W = T_R\Big|_{z=\pm h/2}; \quad r > 0,\, t > 0. \tag{D.3}$$

The fluid velocity term, v, dictates the growing area of fracture infiltrated by the injectate over time. Outside this infiltrated region the fluid temperature gradient, $\partial T_W/\partial r$ must be zero as the thermal conduction in the injectate is negligible. We assume that injectate pressures will be small compared to the compressive strength of the pore space - pore fluid ensemble, *i.e.*$p \ll 1/\beta$, so that flow properties can be treated as independent of pressure changes, we can therefore write

$$v\frac{\partial T_W}{\partial r} \rightarrow \frac{\dot{m}_{r_b}}{2\pi r h \rho_w \phi}\frac{\partial T_W}{\partial r}. \tag{D.4}$$

We then take the Laplace transforms of equations (D.1), (D.2) and (D.3), where we use the notation $\mathcal{L}[X(s)] = \bar{X}(t)$, $\mathcal{L}^{-1}[\bar{X}(s)] = X(t)$.

$$\frac{\partial^2 \bar{T}_R}{\partial z^2} - \frac{s}{\kappa}\bar{T}_R = 0 \tag{D.5}$$

$$\xi s\bar{T}_W + \frac{\dot{m}_{r_b}}{4c_D\pi h\rho_w\phi}\frac{\partial \bar{T}_W}{\partial r} = \frac{2K}{h\phi\rho_w c_w}\frac{\partial \bar{T}_R}{\partial z}\Bigg|_{z=\pm h/2}; \quad r>0,\ t>0 \tag{D.6}$$

$$\bar{T}_W = \bar{T}_R\Big|_{z=\pm h/2}; \quad r>0,\ t>0 \tag{D.7}$$

Solving for $\bar{T}_W$ and $\bar{T}_R$ gives us

$$\bar{T}_W = -\frac{1}{s}\exp\left[\frac{-\pi h\phi\rho_w r^2}{\dot{m}_{r_b}}\left(s + \frac{2K}{h\phi\rho_w c_w}\sqrt{\frac{s}{\kappa}}\right)\right]; \quad r>0,\ z\le h/2 \tag{D.8}$$

$$\bar{T}_R = \bar{T}_W \exp\left[-\sqrt{\frac{s}{\kappa}}(z-h/2)\right]; \quad r>0,\ z\ge h/2 \tag{D.9}$$

which upon inverting the Laplace transform and scaling for boundary and initial values gives:-

$$\Delta T_R = -\Delta T_0 \operatorname{erfc}\left[\frac{2\pi K r^2 + \dot{m}_{r_b}c_w(|z|-h/2)}{2\dot{m}_{r_b}c_w\sqrt{\kappa\left(t-\frac{\pi h\phi\rho_w\xi r^2}{\dot{m}_{r_b}}\right)}}\right]\times$$
$$H\left(t-\frac{\pi h\phi\rho_w\xi r^2}{\dot{m}_{r_b}}\right); \quad r>0,\ z\ge h/2, \tag{D.10}$$

where T_{R_0} is the initial unperturbed rock temperature, T_{W_0} is the initial temperature

of the injected water and $\Delta T_0 = T_{R_0} - T_{W_0}$. The solution for T_W is merely (D.10) with $z = h/2$.

Appendix G

Assumptions and Applicability to Real Injectors

This section attempts to answer concerns regarding assumptions that have been made along the way. The goal is to show that whilst only a simplified system has been considered, to first order the stress fields determined will be appropriate to practical injection systems in a real geothermal field.

G.1 Temperature Gradients

The temperature perturbation (5.14), was solved by assuming *a priori*that axial temperature gradients are much greater than radial, *i.e.*, $\partial^2 T/\partial z^2 \gg \partial^2 T/\partial r^2 + (1/r)\partial T/\partial r$, and hence we ignore radial heat flow. Because we have neglected radial heat flow, the radial temperature gradients in our solution will in fact be somewhat exagerated, in reality radial heat flow would cause radial gradients to be smoothed and reduced by diffusion. Hence if our estimated temperature function, (5.14), satisfies $\partial^2 T/\partial z^2 \gg \partial^2 T/\partial r^2 + (1/r)\partial T/\partial r$ then our solution is self consistent and we can be confident that our assumption is valid (i.e. if equation (5.14) satifies this condition then so must the true temperature function).

Temperature gradients and hence heat flow are negligible outside our previously defined cooled zone, $Ar^2 + Bz > 2$. Inside the cooled inclusion we can calculate thermal gradients and ascertain the conditions that T_R is consistent with our assumption of heat flow being predominantly fault normal. We find that for an approximate

range of

$$\frac{4C^{5/2}\sqrt{\kappa}}{a^2} < t < \frac{1}{2^{10}a^2\kappa^2} \tag{G.1}$$

the assumption holds true. The lower time bound is sensitive to C and for our chosen parameters this is less than 1 second. It should be noted that for times less than these, those regions where the thermal flow is not predominantly fault normal are negligible in terms of the total heat flux they account for. The upper time bound is over 1,000 years. For our *typical injector* it is apparent that the assumptions we make about heat flow are valid.

G.2 Water Expansion

We now turn to estimating the errors introduced by our assumption that the water density is constant with temperature. Even whilst remaining in the liquid phase the pore fluid can undergo appreciable thermal expansion and so cause increased pore pressure. We can gain some idea of the size of this effect by including this behaviour into the pressure diffusion equation (5.2) We write this modified diffusion equation as

$$\frac{\partial^2 p}{\partial r^2} + \frac{1}{r}\frac{\partial p}{\partial r} = \frac{1}{c_D}\left[\frac{\partial p}{\partial t} - \frac{\alpha_w}{\beta}\frac{\partial T_W}{\partial t}\right]. \tag{G.2}$$

The thermal expansion coefficient of the pore water, α_w, is itself a function of temperature but a generous upper bound is given by 10^{-3}. A simple dimensional analysis using the solutions for pressure and temperature already found, equations (5.8) and (5.14), indicates that the thermal expansion term can become a significant source of pressure perturbation in (G.2), though only in the far field where pressures are small, $r \gtrsim (\dot{m}_{r_b}^2 \eta_w \beta c_w \sqrt{\kappa t})/(4\pi^{\frac{3}{2}} \rho_w k h \alpha_w K)$. However, this merits further investigation as to how large an integrated effect this will have on our calculated pressure function, (5.8).

Rather than attempt to solve the now coupled set of equations relating pore pressure and temperature we merely postulate that the total pressure difference is small and look for a discrepancy. *i.e.*we shall continue to assume that the solutions

for pressure and temperature, equations (5.8) and (5.14), are valid, we then integrate equation (G.2) to solve for the perturbed pressure and compare this to equation (5.8). If the comparison shows no significant difference between the two solutions then our postulate is correct. Hence if our postulate is correct then

$$p(r,t) \gg \frac{\alpha_f}{c_D \beta} \left| \int_0^r \frac{1}{r'} \int_0^{r'} r'' \frac{\partial T_W(r'',t)}{\partial t} \partial r'' \, \partial r' \right| \tag{G.3}$$

where $p(r,t)$ is equal to the solution given in (5.8); $T_W(r'',t)$ is (5.14) and r', r'' are simply dummy variables.

In general the right side of (G.3) can be found by quadrature and the inequality tested. However, for the case where $t \gg Cr_c^2$ we can make use of the simplified temperature description (5.17). This allows us to express the right side of (G.3) in closed form as

$$\int_0^r \frac{1}{r'} \int_0^{r'} r'' \frac{\partial T_W(r'',t)}{\partial t} \partial r'' \, \partial r' =$$

$$(T_{R_0} - T_{W_0}) \left(-\frac{E_1\left[\frac{a^2 r'^4}{t}\right]}{16a\sqrt{\pi t}} - \frac{\ln r}{4a\sqrt{\pi t}} - \frac{\gamma}{16a\sqrt{\pi t}} - \frac{\ln\left(\frac{a^2}{t}\right)}{16a\sqrt{\pi t}} \right) \tag{G.4}$$

where γ is Euler's constant (0.57721566...). Whether we use this closed form solution or numeric quadrature to calculate the pressure perturbation we find that for all realistic cases it is always several orders of magnitude less than $p(r,t)$. The effect of the thermal expansion of water on fluid pressure and thermal stress is therefore negligible.

G.3 Steam Filled Fractures; Gas Saturation State

In our derivation of the pore pressure we neglected the possibility of the initial pore fluid in the fracture being steam. Several steam dominated geothermal reservoirs commercially exploited and are known to be seismically active *e.g.* Laderello, The

Geysers. To understand what effect this might have on our solutions we begin by considering the case of a steam filled fracture at gas saturation temperature (*i.e.*pure dry steam at boiling pressure-temperature). In this instance all we have to consider is the pressure increase produced in the steam component due to the emplaced volume of injectate; the injectate will not boil because it only just reaches the boiling temperature applicable to a slightly lower pressure state. We match pressures between the liquid injectate and initial steam at $r = r_i$, where r_i is the injectate infiltration radius. To differentiate between the parameters that vary for water and steam phases we subscript them with $_w$ for water and $_s$ for steam. We have already stipulated that $p_{max} \ll 1/\beta$ which allows us to ignore second order effects of pressure. Solving (5.2) subject to these conditions and (5.7) gives

$$p(r,t) = \frac{\dot{m}_{r_b}}{4\pi\rho_0 kh}\left[\eta_w E_1\left(\frac{r^2}{4c_{D_w}t}\right) - \eta_w E_1\left(\frac{r_i^2}{4c_{D_w}t}\right) + \eta_s E_1\left(\frac{r_i^2}{4c_{D_s}t}\right)\right] H(r_i - r) + \eta_s E_1\left(\frac{r^2}{4c_{D_s}t}\right) H(r - r_i) + p_0 \;\; ; \;\; r \geq r_b,\ |z| \leq h/2,\ t \geq 0 \qquad \text{(G.5)}$$

Note that any increase in pressure in the steam phase at its saturation point leads to transition to a two-phase or superheated state, however, only a tiny quatity of liquid phase will be condensed and the effect on properties will be negligible. The behaviour is always such as to yield a small reduction in injection pressures, for our typical injector the reduction in pressure in the near field is at most 0.5 MPa. There is no effect on fluid flux in the injectate zone and hence no change in the temperature or thermal stress functions already found. Thus the presence of steam at gas saturation conditions reduces the significance of hydraulic pressures compared to thermal stresses.

G.4 Steam Filled Fractures; Superheated State

For the case where the steam is superheated (*e.g.* , The Geysers, Larderello) we have to consider the boiling of the injectate. An approximate solution for the temperature

perturbation for this problem is given in Chapter 6. This makes use of the fact that the latent heat of vaporisation, L_v, is large compared to the specific heat capacities of either water or steam, c_w and c_s, *i.e.*the energy required to change water to steam would lead to a very large temperature change in either of the single phases. However, the details of the derivation are not necessary to give us a useful bound on the thermal stress perturbation.

Figure 5-9 is a schematic plot showing the temperature of the fracture fluids in a superheated fracture as a function of radius. The front of the injectate will always be at the initial temperature of the rock T_{R_0}, see equation (5.14). So that if the fracture is initially full of superheated steam the injectate front will similarly be superheated steam (we are assuming that pressures at the injectate front will not be great enough to induce condensation). Behind this front will be a train of progresively cooler steam. At some point the steam temperatures will have declined to boiling temperatures for the ambient pressure conditions, and behind this point in the moving injectate further energy loss is translated into a change of phase rather than a drop in temperature. This infiltrating zone of two phase fluid is large in radial extent because the amount of energy required to vaporize water, L_v, equates to a very large temperature change for the same mass of single phase steam or water *i.e.*$L_v/c_s \approx 2000$ K, $L_v/c_w \approx 400$ K. Because so much energy is required for the phase change, the infiltrating zone of two phase fluid extracts a large amount of heat from the rock. Evaporative cooling is a very effective method of heat transfer, however, at most the two-phase injectate can only cool down the rock to the boiling temperature for water at ambient reservoir pressures, T_{b_0}. (Note: curiously as the pressure must decrease montonically with radius, so the boiling temperature of the two phase injectate must drop slightly, even whilst the enthalpy increases.)

All the injectate (bar an inifinitesimal quantity at the start) initially enters the fracture as liquid water. So at most we can consider the fracture to have been pre-cooled by the infiltrating zones of steam and two phase fluid to a temperature equivalent to boiling temperature at ambient reservoir pressures, T_{b_0}. The maximum thermal stresses are inversely proportional to the aspect ratio of the cooled zone, *c.f.* Eshelby inclusions [*Eshelby*, 1957]. Therefore from the viewpoint of thermal stress

perturbation, we can form a conservative lower bound by considering the problem as equivalent to injecting water into a fracture where $T_{R_0} = T_{b_0}$. This will have the effect of directly scaling $\Delta\sigma_{zz}$ by $(T_b - T_{W_0})/(T_{R_0} - T_{W_0})$.

For the case of The Geysers, which has some highly underpressured fractures where $p_0 \approx 1$ MPa and $T_{R_0} \lesssim 240°C$, $T_{W_0} \leq 40°C$, this will still lead to $T_b = 180°C$ and stress perturbations at least 0.7 times those calculated in figure 5-5.

For a horizontal fracture we therefore expect to see similar behaviour whether it be steam or liquid filled. However a tilted fracture will introduce buoyancy effects. Where the initial fracture fluid density is similar to the injectate density these effects are small. But for cases where the initial fluid is a steam phase and hence a large density difference exists a large negative buoyancy will act on the injectate and it will tend to flow downhill. We discuss this next.

G.5 Sloping Fractures

If there is a density difference between the injectate and the original fracture fluid, and the fracture is not horizontal, then buoyancy forces will come into play. The force acting on each unit volume of the injectate, downslope in the plane of the fracture is $\Delta\rho \sin\psi g$, where $\Delta\rho$ is the density of the injectate minus the density of the initial fracture fluid; ψ is the dip angle of the fracture; and g is acceleration due to gravity. The flow velocity of the injectate purely due to buoyancy forces, $v_{\rm bf}$ can then be derived from Darcy's law, equation (5.6), to give $v_{\rm bf} = k\Delta\rho \sin\psi g/\eta$. Hence the injectate pressure within the fracture will be controlled by the superposition of radial pressure diffusion and constant downslope flow. The solution of this diffusion problem is discussed in Carslaw and Jaeger [1959, sec 10.7]. The pressure field evolves towards a steady state with time, $t \gg 4c_D/v_{\rm bf}$, given by

$$p(r,t) = \frac{\dot{m}_{r_b}\eta}{2\pi\rho_0 kh} \exp\left(\frac{v_{\rm bf}x}{2c_D}\right) K_0\left(\frac{v_{\rm bf}r}{2c_D}\right) \qquad r \geq r_b,\ |z| \leq h/2,\ t \geq 0. \qquad \text{(G.6)}$$

Here x is distance in the downdip direction and K_0 is the zero'th order modified

Bessel function of the second kind.

The general result is that injectate pressures in a dipping fracture are lower than in a horizontal one. The pressure and flow field though, can be seen to remain essentially radially symmetric in the domain $r << 2c_D/v_{bf}$, which for for our typical injector and maximum $\Delta\rho$ of ~ 1000 kg m^{-3} yields a domain on the order of hundreds of metres about the borehole. The diffusive nature of the solutions means that this will remain true even if the apparent source, (*i.e.*the locus of intersection between borehole and fracture) is no longer circular, as long as it is small compared to diffusive length scale $\sqrt{4c_D t}$. This means that even when injecting water into a near vertical steam filled fracture, with typical injection parameters, the mass flow remains essentially the same as for a horizontal fracture for hundred of metres about the borehole.

The temperature perturbation, and hence the thermal stresses are sensitive only to the mass flow rate of the injectate. And the mass flow rate remains essentially radially symmetric for our typical parameters within a few hundred of metres of the well. For the injection scenarios of interest here the temperature perturbation is restricted to within a few hundred meters about the borehole. Hence the conclusion is that for sloping fractures and typical injection parameters the cooled zone and thermal stresses remain unchanged while overpressures required to drive injection are reduced.

However, it is not unreasonable for conductive fractures to have permeabilities orders of magnitude higher than the rather conservative values we have used in this study. In such an instance the loss of radial symmetry in the mass flow will be apparent closer to the borehole and the temperature perturbation will become distorted downslope. In the Discussion section we show how conservation of energy dictates that the fracture normal length scale and the fracture area of the cooled zone remains constant. Analogy with Eshelby inclusion theory [Eshelby, 1957] indicates that as the cooled zone becomes distorted and radially asymmetric the fracture normal stress perturbation actually increases. Hence sloping fractures tend to decrease the hydraulic injection pressure and increase the thermal stress perturbation.

Bibliography

Abercrombie, R., & P. Leary, Source parameters of small earthquakes recorded at 2.5 km depth, Cajon Pass, southern California: implications for earthquake scaling. *Geophys. Res Lett.*, 20:1511–1514, 1993.

Abramowitz M., & I. Stegun. *Handbook of Mathematical Functions.* Dover Publications, Inc., NY, USA, 1972.

Allen, R.V., Automatic phase pickers: their present use and future prospects. *Bulletin of the Seismological Society of America*, 72:S225–S242, 1982.

Allis, R.G., Mechanism of induced seismicity at the Geysers geothermal reservoir, California. *Geophysical Research Letters*, 9:629–632, 1982.

Arnadottir, T., P. Segall & M. Matthews, Resolving the discrepancy between geodetic and seismic fault models for the 1989 Loma Prieta, California, earthquake, *Bull. Seismol. Soc. Am., 82*, 2248–2255, 1992.

Barker, B.J., M.S. Gulati, M.A. Bryan & K.L. Reidel, Geysers reservoir performance. In *Monograph on the Geysers geothermal field, Special report no. 17*, pages 167–178. Geothermal Resources Council, 1992.

Batini, F., R. Console & G. Luongo. Seismological study of Larderello-Travale geothermal area. pressure and stresses and application to Lake Oroville. *Geothermics*, 14:255–272, 1985.

Bear, J., *Hydraulics of Groundwater.* McGraw-Hill Inc., USA, 1979.

Bendat, J.S., & A.G. Piersol, *Measurement and Analysis of Random Data.* John Wiley & Sons, Inc. New York, 1966.

Bodvarsson, G., Thermal Problems in the Siting of Reinjection Wells. *Geothermics* 1:63–66, 1972.

Boley B.A., & J.H. Weiner. *Theory fo Thermal Stress.* John Wiley & Sons, Inc., New York, USA, 1960.

Bromley, C.J., C.J. Pearson & D.M. Rigor Jr. Microearthquakes at the Puhagan geothermal field, Philippines; a case of induced seismicity. *J. of Volcanology and Geothermal Research* 31:293–311, 1987.

Bufe, C.G., S.M. Marks, F.W. Lester, R.S. Ludwin & M.C. Stickney, Seismicity of The Geysers–Clear Lake region. In *Research in The Geysers-Clear Lake geothermal area, northern California.* Geological survey professional paper 1141, United States Government printing office, 1981.

Byrd, P.F., & M.D. Friedman *Handbook of Elliptic Integrals for Engineers and Scientists, 2nd ed., rev.* Springer-Verlag, Berlin, 1971.

California Division of Oil, Gas and Geothermal Resources (DOGGR), The Geysers geothermal field (map) In *Monograph on the Geysers geothermal field, Special report no. 17,* Attachment. Geothermal Resources Council, 1992.

Carslaw, H.S., & J.C. Jaegar. *Conduction of Heat in Solids.* Oxford Science Publications, Oxford, U.K., 1959.

Cornet, F.H., J. Helm, H. Poitrenaud & A. Etchecopar, Seismic and aseismic slips induced by large-scale fluid injections, *Pageoph.* 150:563–583, 1997.

Chasteen, A.J., Geothermal Steam Condensate Reinjection. *Proceedings Second United Nations Symposium on the Development and Use of Geothermal Resources,* v2:1335–1336, 1975.

David, C., T. Wong, W. Zhu & J. Zhang, Laboratory Measurement of Compaction–induced Permeability Change in Porous Rocks: Implications for the Generation and Maintenance of Pore Pressure Excess in the Crust *Pageoph.*, 143:425–456, 1994.

Denlinger, R.P., W.P. Isherwood & R.L. Kovach, Geodetic analysis of reservoir depletion at The Geysers steam field in northern California. *Journal of Geophysical Research*, 86:6091–6096, 1981.

Denlinger, R.P., & C.G. Bufe, Reservoir conditions related to induced seismicity at The Geysers steam reservoir, northern California. *Bulletin of the Seismological Society of America*, 72:1317–1327, 1982.

Dieterich, J.H., A constitutive law for rate of earthquake production and its application to earthquake clustering. *Journal of Geophysical Research*, 99:2601–2618, 1994.

Dieterich, J.H., & B. Kilgore, Implications of fault constitutive properties for earthquake prediction. *Proc. Natl. Acad. Sci. USA* 93:3787–3794, 1996.

Diggle, P.J., *Time Series A Biostatistical Introduction.* Oxford University Press. U.K., 1990.

Eason, G., B. Noble & I.N. Sneddon, On certain integrals of lipschitz-hankel type involving products of bessel functions. *Phil. Trans. Royal Soc. London (A)*, 247:529–551, 1955.

Eaton, J.P., Determination of amplitude and duration magnitudes and site residuals from short-period seismographs in northern California. *Seismological Society of America Bulletin*, 82:533–579, 1992.

Eberhart-Phillips, D., & D.H. Oppenheimer, Induced seismicity in The Geysers geothermal area, California. *Journal of Geophysical Research*, 89:1191–1207, 1984.

Efron, B., & R.J. Tibshirani, *An Introduction to the Bootstrap.* Chapman & Hall, New York, U.S.A., 1993.

Eshelby, J.D., The determination of the elastic field of an ellipsoidal inclusion and related problems. *Proc. R. Soc. Lond.* A241:376–396, 1957.

Evans, K.F., T. Kohl, L. Rybach & R.J. Hopkirk, The effects of fracture normal compliance on the long term circulation behavior of a hot dry rock reservoir: a parameter study using the new fully–coupled code 'FRACTure'. *Geothermal Resources Council Transactions*, 16:449–456, 1992.

Evans, K.F., T. Kohl, R.J. Hopkirk & L. Rybach, *Modelling of energy production from Hot Dry Rock systems.* Nationaler Energie-Forschungs-Fonds Projekt 359 – Final Report, 316 pp, Inst. of Geophys., Swiss Federal Inst. of Tech., Zurich, Switzeland, April 1992. Modelling of energy production from Hot Dry Rock systems. *Report to Swiss National Energy Research Fund*, NEFF No. 359, April 1992.

Fitzgerald S.D., K. Pruess & D.M. Van Rappard, Laboratory studies of injection into horizontal fractures, *Proc. 21st Workshop on Geothermal Reservoir Engineering.*, Stanford, 355-360, 1997.

Fitzgerald S.D., C.T. Wang & K. Pruess, Laboratory and Theoretical Studies of Injection into Horizontal fractures. *Proc. New Zealand Geothermal Workshop*, 18:267–273, 1996.

Fuller, W.A., *Introduction to Statistical Time Series.* John Wiley, N.Y., U.S.A., 1976.

GRL Special Edition, Editor Geller, R.J., Debate on "VAN". *Geophys. Res Lett.*, 23:1291–1452, 1996.

Gunderson, R.P., Porosity of reservoir graywacke at The Geysers. In *Monograph on the Geysers geothermal field, Special report no. 17*, pages 89–93. Geothermal Resources Council, 1992.

Habermann, R.E., Comparison of Berkeley and Calnet magnitude estimates as a means of evaluating temporal consistency of magnitudes in California. *Seismological Society of America Bulletin*, 78:1255–1267, 1988.

Healy, J.H., W.W. Rubey, D.T. Griggs & C.B. Raleigh. The denver earthquakes. *Science*, 161:1301–1310, 1968.

Henley, R.W., A.H Truesdell & P.B. Barton Jr., *Fluid–Mineral Equilibria in Hydrothermal Systems. Reviews in Economic Geology, Vol. 1.* Society of Economic Geologists, 1984

Hill, D., J.P. Eaton & L.M. Jones, Seismicity, 1980-86. In *The San Andreas Fault System, California.* U.S. Geological Survey Professional Paper 1515, Washington, D.C., 1990.

Hofmann-Wellenhof, B., H. Lichtenegger & J. Collins, *GPS Theory and Practice*, 3rd rev. ed., Springer-Verlag, Wien, 1994.

Hubbert, M.K., & W.W. Rubey, Mechanics of fluid-filled porous solids and its application to overthrust faulting, [Pt.] 1 of Role of fluid pressure in mechanics of overthrust faulting. In *Geol. Soc. Am. Bull.,* v. 70, no. 2, p. 115-166, illus., Feb. 1959)

Kagan, Y.Y., VAN earthquake predictions – an attempt at statistical evaluation. *Geophys. Res Lett.*, 23:1315–1318, 1996.

Kern, H., Elastic Wave Velocities and Constants of Elasticity of Rocks at Elevated Pressures and Temperatures. In *Physical Properties of Rocks, Vol 1b.* Ed. Angenheister, Springer–Verlag, 1982.

Klein, F.W., User's guide to HYPOINVERSE, a program for VAX computers to solve for earthquake locations and magnitudes. In *U.S. Geol. Surv. Open-File Report 89-314*, 61., 1989.

Kozeny, J., Uber Kapillare Leitung des Wassers im Boden. *Sitz-Ber. Weiner Akad.*, IIa, 136:271–306,1927

Landau L.D. & E.M. Lifshitz, *Fluid Mechanics*, Pergamon Press, Oxford, U.K., 1959.

Langbein, J., F. Wyatt, H. Johnson, D. Harmann & P. Zimmer, Improved stability of a deeply anchored geodetic monument for deformation monitoring, *Geophys. Res Lett., 22*, 3533–3536, 1995.

Leick, A., *GPS Satellite Surveying, 2nd edition* Wiley–Interscience, New York, 1992.

Lofgren, B.E., Monitoring crustal deformation in the geyser-clear lake region. In *Research in The Geysers-Clear Lake geothermal area, northern California.* Geological survey professional paper 1141, United States Government printing office, 1981.

Majer, E.L., & T.V. McEvilly, Seismological investigations at the geysers geothermal field. *Geophysics*, 44:246–269, 1979.

Majer, E.L., R.H. Chapman, W.D. Stanley & B.D. Rodriguez, Geophysics at the Geysers. In *Monograph on The Geysers geothermal field, Special report no. 17*, pages 97–110. Geothermal Resources Council, 1992.

Matthews, M.V., & P. Segall, Estimation of depth-dependent fault slip from measured surface deformation with application to the 1906 San Francisco earthquake, *J. Geophys. Res., 98*, 12153–12163, 1993.

Mavko, G., T. Mukerji & J. Dvorkin, *Rock Physics Handbook.* Rock Physics Laboratory, Stanford University, 1996.

Menzies, A.J., & M. Pham, A field–wide numerical simulation model of The Geysers geothermal field, California, USA. In *Proc. World Geothermal Congress, 1995*, 3:1697–1702, 1995.

Milbert, D.G., & D.A. Smith, Converting GPS height into NAVD88 elevation with the GEOID96 geoid height model, in *Proceedings of GIS/LIS '96 Annual Conference and Exposition, Denver,* pp. 681–692, Am. Congr. on Surv. and Mapp., Washington, D.C., 1996.

Mogi, K., Relations Between Eruptions of Various Volcanoes and the Deformation of the Ground Surface Around Them. *Bull. Earthquake Res. Inst. Univ Tokyo*, 36:99–134, 1958.

Mossop A. and P. Segall. Induced Seismicity at The Geysers, Northern California. *Eos Trans. AGU,* 75 (44), 444, 1994.

Mossop A. and P. Segall. Stresses Induced by Injection of Cold Fluids into Hot Fractured Rock. *Eos Trans. AGU,* 76 (46), F354, 1995.

A.P. Mossop and P. Segall, Subsidence at The Geysers geothermal field, N. California from a comparison of GPS and leveling surveys. *Geophys. Res Lett.*, 24:1839–1842, 1997.

A.P. Mossop and P. Segall. Volume strain within The Geysers geothermal field. *J. Geophys. Res.*, , 104:29113–29131, 1999.

A.P. Mossop and P. Segall. Induced seismicity in geothermal fields: I – a thermoelastic injection model. *submitted J. Geophys. Res.,* July 2000.

Murray, M.H., G.A. Marshall, M. Lisowski & R.S. Stein, The 1992 M=7 Cape Mendocino, California, earthquake: Coseismic deformation at the south end of the Cascadia megathrust. *Journal of Geophysical Research*, 101:17707–17725, 1996.

Nowacki, W., *Thermoelasticity.* Pergamon Press, Oxford, 1962.

Nur A., & J.D. Byerlee, An Exact Effective Stress Law for Elastic Deformation of Rock with Fluids. *Journal of Geophysical Research*, 76:6414–6419, 1971.

O'Connell, D.R.H., & L.R. Johnson, Progressive inversion for hypocentres and P wave and S wave velocity structure: application to the Geysers, California, geothermal field. *Journal of Geophysical Research*, 96:6223–6236, 1991.

Okada, Y., Internal deformation due to shear and tensile faults in a half-space, *Bull. Seismol. Soc. Am., 82*, 1018–1040, 1992.

Oppenheimer, D.H., extensional tectonics at The Geysers geothermal area, California. *Journal of Geophysical Research*, 91:11,463–11,476, 1986.

Oppenheimer, D.H., F. Klein, J. Eaton & F. Lester, The Northern California Seismic Network Bulletin January-December 1992. In *U.S. Geol. Surv. Open-File Report 93-578*, 45pp., 1993.

Parker, R.L., *Geophysical Inverse Theory*, Princeton Univ. Press, Princeton, N.J.,1994.

Press, W.H., B.P. Flannery, S.A. Teukolsky & W.T. Vetterling, *Numerical Recipes.* Cambridge University Press, 1989.

TOUGH User's Guide, Earth Sci. Div., Report LBL-20700, Lawrence Berkeley Laboratory, 1991.

Pugh, E.M., & G.H. Winslow, *The Analysis of Physical Measurements.* Addison-Wesley, 1966.

Raleigh, C.B., J.H. Healy & J.D. Bredehoeft, Faulting and crustal stress at rangely, colorado. In *Flow and fracture of rocks (Griggs volume)*, pages 275–284. American Geophysical Union Geophysical Monograph 16, Washington, D.C., 1972.

Reasenberg, P., Second-order moment of central California seismicity, 1969–1982. *Journal of Geophysical Research*, 90:5479–5495, 1985.

Segall, P., Earthquakes triggered by fluid extraction. *Geology*, 17:942–946, 1989.

Segall, P., Induced stresses due to fluid extraction from axisymmetric reservoirs. *Pageoph*, 139:535–560, 1992.

Segall, P., & S. Fitzgerald, A note on induced stress changes in hydrocarbon and geothermal reservoirs. *Tectonophysics* 289:117–128, 1998.

Sherburn, S., Seismic monitoring during a cold water injection experiment, Wairakei geothermal field: preliminary results. In *Proc. New Zealand Geothermal Workshop*, 6:129–133, 1984.

Stark, M.A., Imaging injected water in the Geysers reservoir using microearthquake data. In *Geothermal Resources Council Transactions*, vol.14 part II: 1697–1704, 1990.

Stark, M.A., Microearthquakes – a tool to track injected water in The Geysers reservoir. In *Monograph on the Geysers geothermal field, Special report no. 17*, pages 111–117. Geothermal Resources Council, 1992.

Stark, P.B., A few considerations for ascribing statistical significance to earthquake predictions. *Geophys. Res Lett.*, 23:1399–1402, 1996.

Taylor, R.E., R.L. Shoemaker & H. Groot, Thermophysical Properties of Selected Rocks: A Report to U.S. Geological Survey. *TPRL 271* 32 pp., Thermophysical Prop. Res. Lab., Purdue Univ., Ind., 1982.

Theis, C.V., The relation between the lowering of the piezometric surface and the rate and duration of a well using groundwater storage. *Trans. AGU*, 2:519-524, 1935.

Thompson, R.C., Structural stratigraphy and intrusive rocks at The Geysers geothermal field. In *Monograph on the Geysers geothermal field, Special report no. 17*, pages 59–64. Geothermal Resources Council, 1992.

Truesdell, A.H., J.R. Haizlip, W.T. Box & F. D'Amore, A geochemical overview of The Geysers geothermal reservoir. In *Monograph on the Geysers geothermal field, Special report no. 17*, pages 121–132. Geothermal Resources Council, 1992.

Wahba, G., *Spline Models for Observational Data*, Soc. for Ind. and Appl. Math., Philadelphia, Pa., 1990.

Walters, M.A., & J. Combs, Heat flow in The Geysers–Clear Lake geothermal area of nothern California, U.S.A. In *Monograph on The Geysers geothermal field, Special report no. 17*, pages 43–53. Geothermal Resources Council, 1992.

Webb, F.H., & J.F. Zumberge, An Introduction to GIPSY/OASIS–II, *Rep. JPL D–11088*, Jet Propul. Lab., Pasadena, Calif., 1995.

Williamson, K.H., Reservoir Simulation of The Geysers Geothermal Field. *Proc. 15th Workshop on Geothermal Reservoir Engineering.*, Stanfoord, 355-360, 1990.

Williamson, K.H., Development of a Reservoir Model for The Geysers geothermal field. In *Monograph on the Geysers geothermal field, Special report no. 17*, pages 179–187. Geothermal Resources Council, 1992.

Zhang, J., Y. Bock, H. Johnson, P. Fang, S. Williams, J. Genrich, S. Wdowinsk & J. Behr, Southern California permanent GPS geodetic array: Error analysis of daily position estimates and site velocities. *J. Geophys. Res., 102*, 18035–18055, 1997.